Analog Explorations of Quantum State Measurement

Benjamin Krawciw and James P. Crutchfield
Complexity Sciences Center and Department of Astronomy and Physics
University of California at Davis, One Shields Avenue, Davis, CA 95616
(Dated: November 23, 2026)

The awkward disconnect in the postulates of quantum mechanics between the continuous, deterministic, linear, and unitary evolution governed by Schrödinger's equation and the discontinuous, stochastic, nonlinear, and nonunitary measurement process has vexed physicists for decades. Intuition from classical mechanics, statistical mechanics, and dynamical systems theory suggests that such a process might be modeled with a nonlinear system of differential equations. We explore such approaches by designing a deterministic model of an ideal projective measurement on a single qubit and constructing an analog computer that simulates it by manipulating voltages in an electrical circuit. The model reduces to Schrödinger evolution when no measurement is taking place. During a measurement, a hidden variable that the observer does not resolve selects the outcome, and the model is constructed so that a uniformly distributed hidden variable yields Born-rule frequencies. We do not derive the Born rule; rather, we show that a deterministic dynamical system with no intrinsic noise can implement it. Over 300 trials, the circuit reproduces the ideal model's individual outcomes to within one percent of the decision threshold, and its outcome frequencies match the Born rule to within about 0.02 in probability. These results are a small but provocative step towards modeling quantum measurement with macro-scale machines—a step of interest for both the foundations of physics and the alternatives to digital computing it suggests.

Keywords: quantum measurement, analog computation, Born rule, single qubit

arXiv:2611.26889v1 [quant-ph] 19 Nov 2026

I. INTRODUCTION

We explore deterministic dynamics that bridge the gap between Schrödinger time evolution and randomized state collapse during a measurement by building an analog computer that simulates measurement on a single qubit.

It is worth stating at the outset what this does and does not show. We construct a deterministic, nonlinear model of an ideal projective measurement of a single qubit and build an electrical circuit that implements it. In the model, which outcome occurs is decided by a hidden variable ϕ that the observer does not resolve. The Born rule enters by design: we choose how the outcome depends on ϕ so that, when ϕ is uniformly distributed from the observer's point of view, the outcome frequencies are those of the Born rule.

We therefore do not claim to derive the Born rule nor to have found the physical mechanism behind it. Nor do we identify ϕ with a particular quantum-mechanical degree of freedom. In both the model and the circuit it is an engineered, unresolved variable. (That said, Section VII speculates about to what it might correspond.) What the model does demonstrate is that a single deterministic dynamical system can reduce to Schrödinger evolution when no measurement occurs and produce definite outcomes with Born-rule statistics when one does. It does this without any intrinsic source of noise, in contrast to the stochastic collapse theories reviewed below.

Reproducing single-qubit Born-rule statistics with a hidden variable is not itself new [1, 2]. With a uniformly distributed hidden variable it is straightforward. What is new here is how the outcome comes about. Collapse is a finite-time trajectory of a single deterministic, noise-free system of differential equations, with no separate rule for measurement. A measurement is simply a coupling that is switched on. And the equations are simple enough, polynomial in the state, to build as an electronic circuit, in which the intermediate states of a collapse are voltages that can be recorded. We treat only ideal projective measurements. Weak measurements and general positive operator-valued measures (POVMs) are beyond our present scope.

There are several parallel motivations: First, we are interested in these dynamics as a possible avenue for resolving the longstanding measurement problem—viz., the disconnect between Schrödinger time evolution and measurement. Second, the simulation of quantum problems on an analog computer is interesting from a modern technological point of view. Even if deterministic dynamics are ultimately unsatisfying as a resolution to the measurement problem, it may still make for a useful and interesting method to simulate quantum phenomena. Finally, there are pedagogical benefits. To get started, the next section briefly reviews the measurement problem and the use of analog computers for simulating quantum phenomena.

II. BACKGROUND

The following first reviews basic quantum theory and quantum measurement. It then reviews various alternative, even contemporary, views on the role of measurement, including wave function collapse theories and the dynamical role of decoherence.

A. Postulates of Quantum Mechanics

For our purposes, the postulates of quantum mechanics [3, p. 166] can be summarized as follows:

1. *State*: A quantum system's state is given by a normalized ket vector $|\psi\rangle$ in a Hilbert space $\mathcal{H}$. Normalized superpositions of states are also possible states. For a qubit $\mathcal{H} = \mathbb{C}^2$, so the state is a pair of complex amplitudes.

2. *Dynamic*: Unless the system is being measured, the state evolves over time according to the Schrödinger differential equation:

$$i\hbar \frac{d}{dt} |\psi\rangle = \widehat{H} |\psi\rangle , \tag{1}$$

where $\widehat{H}$ is the system Hamiltonian—a linear and Hermitian operator. The resulting time evolution is linear and unitary.

3. *Measurement*: A measurable quantity A is associated with a linear Hermitian operator $\widehat{A}$, whose eigenvectors form an orthonormal basis. When A is measured, the outcome is one of $\widehat{A}$'s eigenvalues a_n decided at random and the state collapses to the corresponding normalized eigenstate $|v_n\rangle$. The probability of this outcome is given by the Born Rule:

$$P(a_n) = |\langle \psi | v_n \rangle|^2 \ . \tag{2}$$

(For a degenerate eigenvalue the state is instead projected onto the corresponding eigenspace and renormalized. A single qubit measured in a basis never requires this case.)

B. The Measurement Problem

The measurement problem is this: The Schrödinger and measurement postulates give competing rules for how a quantum state evolves over time, and there is no clear objective criterion to decide which to use at any given moment.

It is useful to split this into two parts. The first is to say what a measurement is: which physical processes count as measurements, and how they can depart from Schrödinger evolution. The second is to say which outcome occurs: once a measurement has taken place, what selects the single result that the observer records? As we will see, unitary quantum mechanics with an environment gives a good answer to the first part, but not the second.

One potential solution would be to harmonize the two postulates. Could measurement be a special case of Schrödinger dynamics? The answer is no, for both closed and open systems. The formal solution to the Schrödinger equation is $|\psi(t)\rangle = \widehat{U}(t) |\psi(0)\rangle$, where:

$$\widehat{U}(t) = \exp\left(\frac{-i}{\hbar}\widehat{H}t\right) \tag{3}$$

is linear and unitary, hence invertible with inverse $\widehat{U}^\dagger(t)$.

For a closed system, measurement violates unitarity. Consider a qubit and the two states $|\alpha\rangle = (|0\rangle + |1\rangle)/\sqrt{2}$ and $|\beta\rangle = (|0\rangle - |1\rangle)/\sqrt{2}$. A measurement in the 0/1 basis may collapse either one to $|0\rangle$. The map is then not invertible, since it is impossible to decide whether $|0\rangle$ came from $|\alpha\rangle$ or $|\beta\rangle$. So, it cannot be unitary and cannot be a solution of the Schrödinger equation.

For an open system, measurement violates linearity. Now, the system is coupled to an environment, and basis states take the form:

$$|0\rangle \otimes |\epsilon_n\rangle \ \text{ or } \ |1\rangle \otimes |\epsilon_n\rangle ,$$

where $|\epsilon_n\rangle$ is a basis state of the environment. If a measurement in the 0/1 basis could be modeled by a unitary evolution $\widehat{U}_M$, then it must leave the eigenstates $|0\rangle$ and $|1\rangle$ of the measurement alone:

$$\begin{aligned} \widehat{U}_M (|0\rangle \otimes |\epsilon\rangle) &= |0\rangle \otimes |\epsilon'\rangle \ \text{ and} \\ \widehat{U}_M (|1\rangle \otimes |\epsilon\rangle) &= |1\rangle \otimes |\epsilon''\rangle , \end{aligned}$$

where $|\epsilon\rangle$, $|\epsilon'\rangle$, and $|\epsilon''\rangle$ are arbitrary environment states. However, any state can be written as $|\psi\rangle = \sum_n a_n |0\rangle \otimes |\epsilon_n\rangle + b_n |1\rangle \otimes |\epsilon_n\rangle$, and by the linearity of $\widehat{U}_M$:

$$\widehat{U}_M |\psi\rangle = \sum_n a_n |0\rangle \otimes |\epsilon'_n\rangle + b_n |1\rangle \otimes |\epsilon''_n\rangle .$$

Superpositions of $|0\rangle$ and $|1\rangle$ therefore survive: $\widehat{U}_M$ entangles the qubit with its environment but does not collapse it. Collapse requires a violation of linearity, so no $\widehat{U}_M$ generated by a linear Hamiltonian can produce a single definite outcome.

This conditional unitary is nonetheless the core of the decoherence program and of Quantum Darwinism, reviewed below. There, a measurement *is* an evolution of the form $\widehat{U}_M$: the environment changes conditioned on the system's pointer states, here $|0\rangle$ and $|1\rangle$, leaving system and environment in a superposition of *branches*, one per outcome [4]. The evolution is invertible on the joint space of system and environment but not on the system alone. This answers the first part of the measurement problem: it says what physical process a measurement is. It does not answer the second. Each branch carries one outcome, but nothing in the unitary dynamics selects which branch the observer finds.

The same linearity underlies the *no-cloning theorem* [5, 6]; see also [7, p. 532]. A map that copies the basis states, $|0\rangle \otimes |e\rangle \to |0\rangle \otimes |0\rangle$ and $|1\rangle \otimes |e\rangle \to |1\rangle \otimes |1\rangle$, must by linearity send a superposition $(A|0\rangle + B|1\rangle) \otimes |e\rangle$ to the entangled state $A|0\rangle \otimes |0\rangle + B|1\rangle \otimes |1\rangle$, not to two

copies of the superposition. So no linear dynamics can copy an unknown state. Dieks framed the result as a rebuttal to a proposed superluminal communicator [6]: if unknown states could be cloned, entanglement could be used to signal. A model of measurement must abandon linearity, by the argument above, and so it also loses this automatic protection against cloning and signaling. It must secure them some other way. We return to this point in Sec. VII.

These closed- and open-system arguments motivate the following design principles. A dynamical model of measurement must (i) reduce to Schrödinger evolution when no measurement is taking place, (ii) be nonlinear and nonunitary while a measurement is taking place, driving every state to one of the measurement's eigenstates, and (iii) select among those eigenstates with Born-rule frequencies.

C. Decoherence and Dynamical Outcome Selection

Despite its unitary-only approach, the decoherence program [8–13] in quantum physics has had remarkable success in explaining several features of measurement through the system's coupling to its environment. In particular, decoherence causes macroscopically-problematic superpositions of states (such as the simultaneously dead and alive Schrödinger's cat) to evolve toward unproblematic *pointer* states (either alive or dead, but not both). These appear to an observer [9, 13] as a statistical mixture of basis states. This mechanism is called *einselection* [10]. Furthermore, *Quantum Darwinism* showed that the Born Rule can be deduced from more modest assumptions about measurement [11, 12]. Particularly noteworthy is the assumption that repeated measurements give the same result; this is essentially state collapse.

Despite these successes, unitary-only quantum mechanics leaves the second part of the measurement problem open. It lacks a complete account of collapse or, empirically equivalently, of which branch an observer ends up in under a many worlds interpretation [8]. In a many worlds interpretation, the wave function of the universe evolves only according to the Schrödinger equation, but an observer perceives only a single "record", which splits into "branches" during the physical processes we interpret as measurements. In any case, the time evolution seen by the observer is necessarily nonunitary.

Resolving the second part requires something beyond unitary quantum mechanics that selects one outcome. We group the proposals that place this selection in the dynamics, rather than in the observer, under the name *dynamical outcome selection*. They come in three kinds: hidden-variable theories without collapse, stochastic objective collapse theories, and deterministic collapse theories. Our model is of the third kind.

The most prominent hidden-variable theory is *pilot wave theory* [14], in which particles with definite positions are pushed along deterministically by a wave that evolves according to the Schrödinger equation without collapse. Strictly speaking, it is not a collapse theory, since the wave never collapses. A measurement sends the particle configuration into one branch of the wave, and the other branches, though still present, no longer affect it. This is sometimes called *effective* collapse. Born Rule probabilities emerge as the statistical description of ensembles of these trajectories [15]. The pilot wave is defined at all points in configuration space simultaneously in a particular reference frame [1], so the theory is explicitly nonlocal. This is what lets it agree with *Bell's theorem* [16]: no *local* hidden-variable theory—one in which each measurement outcome depends only on the setting chosen at that location and on variables fixed in advance—can reproduce all the predictions of quantum mechanics. Bell proved this by bounding the correlations between measurements on two separated systems. In the form usually tested [17], each of two observers measures one member of a pair along one of two settings (a or a', and b or b') and records ± 1. Writing $E(a, b)$ for the average product of the two outcomes, every local hidden-variable theory satisfies *Bell's inequality*:

$$S = |E(a, b) + E(a, b') + E(a', b) - E(a', b')| \leq 2,$$

whereas quantum mechanics predicts $S = 2\sqrt{2}$ for a maximally entangled pair with suitably chosen settings. Experiments find $S > 2$—an observed violation of Bell's inequality—including tests that close the major loopholes [18–21]. Pilot wave theory accommodates this violation, but at the cost of a preferred reference frame—a major paradigm shift whose merits are still debated [15].

The theories in which the wavefunction does collapse are known as *objective collapse theories* [8]. They maintain the ontology of standard quantum mechanics (only states/wavefunctions), but modify the Schrödinger equation to include collapse. The most popular among these are the Ghirardi-Rimini-Weber (GRW) theory [22], the continuous spontaneous localization (CSL) theory [23], and the Diósi-Penrose (DP) theory [24]. GRW describes the wavefunction as evolving according to Schrödinger evolution, except with random "hits" that suddenly localize the wavefunction. CSL builds off GRW by replacing the discrete hits with a continuous Itô stochastic process. While DP proposes spontaneous localization based on gravity. The three models all share that they are stochastic in nature, describing a nondeterministic evolution of the wave function, conceptually similar to Brownian motion.

Our model also modifies the Schrödinger equation, but it contains no noise term. The dynamics are deterministic, and the apparent randomness of outcomes arises entirely from the observer's ignorance of the hidden variable ϕ. Of the two parts of the measurement problem, our model addresses the second. The hidden variable ϕ selects the outcome. We do not derive the first part: in the model, a measurement is the switching on of a coupling to a measurement apparatus, whose physical origin we leave open. This places it closest to the earliest deter-

ministic collapse proposals, which predate the stochastic theories above. Bohm and Bub [2] added a nonlinear term to the Schrödinger equation that reduces the state continuously and deterministically to one outcome, selected by hidden variables; averaging over those variables recovers the usual quantum statistics. Pearle [25] likewise proposed a nonlinear term that rapidly drives the amplitude of one component of a superposition to one and the rest to zero. More general deterministic, nonlinear modifications of quantum mechanics were later proposed by Weinberg [26], and are known to be in tension with relativistic causality [27, 28]. We return to this in Sec. VII.

III. DETERMINISTIC COLLAPSE ON AN ANALOG COMPUTER

Our goal is to explore deterministic collapse theories. Such a theory must share most features of the Schrödinger equation, so that it reduces to it in the non-measurement limit, but it must also generate the apparent randomness and definite outcomes of the measurement postulate. The following develops a theory for a single qubit under measurement. It then builds an analog computer that demonstrates the theory's efficacy at re-creating apparent randomness that arises in measurement.

We build an analog computer for two reasons: First, the analog computer acts as a simulation of the theory, making explorations and testing easier than a purely analytical approach. Second, the analog computer is interesting in its own right. The approach of using one physical system to simulate another analogous system with similar dynamics is old, older than the dominant paradigm today of digital computers. It also underlies Feynman's suggestion for quantum simulation—aka quantum computing [29]. Slide rules, planimeters, and Lord Kelvin's tide predicting machine [30] are canonical examples of these analog computers. Modern research in analog computers [31–33] is often motivated by time complexity. An analog computer can sometimes sidestep lengthy calculations by instead observing the outcome of a physical process that follows the same dynamics.

A particularly enticing possibility is the use of analog computers as an alternative to quantum computers. As noted, Feynman's desiderata for quantum computing was essentially this notion of simulation of quantum phenomena by analogous quantum physical systems [29]. Feynman even highlighted simulating quantum systems by classical probabilistic systems as an interesting possibility. Analog simulation of quantum computers has been explored in the past [34–36]. Focusing only on Schrödinger evolution, none of these previous explorations attempt to model state collapse.

There have been interesting developments in the physical simulation of pilot wave dynamics through oil droplets skittering around on a vibrating fluid surface [37]. This implementation, however, falls in the ontology of pilot wave theory, not standard quantum mechanics.

The current roadblock to using analog computers as an effective substitute for quantum computers is that all existing hardware implementations, including the one we develop here, require explicit construction of the entire Hilbert space. In contrast, a quantum computer with N qubits allows operations on a 2^N dimensional Hilbert space (generated by the tensor product of N 2D spaces) while only requiring the physical construction of N qubits. Probing this concern, our physical implementation of the deterministic collapse model is partly motivated by a desire to discover new ways of encoding a quantum state in an analog system. It is conceivable that a model of state collapse could suggest a method of encoding many dynamical variables in a small number of physical objects, as in a quantum computer.

Our development proceeds as follows. Section IV explains the design of our model. It discusses why the equations of motions are chosen as they are, it summarizes the design of the electrical circuits that implement them as an analog computer. Section V is a bit of a sidebar on analog computers, included to address their likely unfamiliarity. Then, Section VI gives the results of testing this analog computer, which confirm that the device successfully re-creates Born Rule statistics. Finally, Section VII summarizes our results, draws physical implications from them, and discusses the next steps to take in the exploration of these deterministic collapse theories.

IV. METHODS

This section motivates and explains the design of our analog circuit qubit. First, Subsection IV A builds a system of coupled ODEs that simulates a qubit under measurement. The design of these ODEs is constrained to contain only the sorts of operations we can build an analog circuit to perform. Next, Section V discusses analog computer building blocks, giving an understanding of what kinds of behaviors an analog computer built from an electronic circuit can emulate. Finally, Subsection V B gives the full design of the analog computer in the form of block diagrams at the high level and circuit diagrams at the detailed level.

A. Constructing Qubit ODEs

The equations of motion we construct are constrained by the hardware that can solve them. Our analog computer is built from a small repertoire of standard subcircuits, detailed in Subsection VA: they scale voltages by constants, add and subtract them, integrate them over time (with a sign inversion), and multiply pairs of them together. They do not take square roots, exponentials, logarithms, or trigonometric functions. We therefore restrict the right-hand sides of our ODEs to polynomials

in the state variables and parameters. This restriction drives several of the choices below: storing the state in Cartesian coordinates rather than as an angle, enforcing normalization with a restoring force rather than exactly, using second-order equations, and writing the Born-rule probability as a polynomial.

The quantum mechanics reviewed in Section I enters the model at three points. The state, a pair of complex amplitudes, becomes a point (x, y) on the unit circle (Subsection IV C). The orthonormal eigenbasis of the measured observable becomes a pair of antipodal attractors $\pm(c, s)$ (Subsection IV E). And the Born rule becomes the fraction of hidden-variable values that select each attractor (Subsection IV F).

B. Qubit dynamics in standard quantum mechanics

Before building the differential equations, let us discuss the phenomena we are trying to model. We have a single qubit, whose state takes the form:

$$|\psi\rangle = A\,|0\rangle + B\,|1\rangle\,. \tag{4}$$

For normalization, the complex coefficients $A, B \in \mathbb{C}$ must satisfy:

$$|A|^2 + |B|^2 = 1. \tag{5}$$

When the qubit is not being measured, its state evolves in time according to the Schrödinger Equation:

$$i\hbar\frac{d}{dt}\,|\psi\rangle = \widehat{H}\,|\psi\rangle\,. \tag{6}$$

The Hamiltonian $\widehat{H}$ is a linear Hermitian operator, and the solution is:

$$|\psi(t)\rangle = \exp\left(\frac{-i}{\hbar}\widehat{H}t\right)|\psi(0)\rangle\,,$$

where the operator exponential is defined using its power series.

A general Hamiltonian may be split into linear and nonlinear parts. The linear part alone produces unitary evolution, which cannot collapse a state (Subsection II B), so collapse must come from the nonlinear part; that is the part our model constructs, and it is switched on only during a measurement. For ease of modeling we set the linear part to zero, $\widehat{H}_{\text{linear}} = 0$. Little is lost by this choice. The identity component of $\widehat{H}_{\text{linear}}$ only advances the global phase, which we treat separately as a hidden variable (Sec. VII). Of the remaining components, only the one proportional to $\widehat{\sigma}_y$ keeps the amplitudes real and hence the state on the circle of Subsection IV C. It rotates the Bloch sphere rigidly about its y axis, which maps that circle to itself and so rotates the circle rigidly ($\dot{x} = -\Omega y$, $\dot{y} = \Omega x$). It could be added to the circuit with two resistors cross-coupling the x and y integrators. Evolving under it before a measurement is equivalent to preparing a rotated initial state, which our experiments already sweep. The other components introduce a complex relative phase and would require a third state variable. A linear Hamiltonian acting *during* a measurement, competing with the collapse dynamics, is left to future work.

Thus, between measurements, $|\psi\rangle$ is constant. In particular, the state does not evolve toward, or settle at, any special point before a measurement: the pre-measurement state is simply whatever state the qubit was prepared in or left in by the previous measurement. In our experiments (Subsection VI A), it is the state left by the previous measurement, which the controller records and uses to set the next measurement axis.

When a measurement occurs, it is specified by a linear Hermitian operator $\widehat{O}$ called an *observable*. By the spectral theorem, this operator has two orthonormal eigenstates $|\uparrow\rangle$ and $|\downarrow\rangle$. Before the measurement, the qubit is in an arbitrary state $|\psi\rangle$. After the measurement, the qubit is in either $|\uparrow\rangle$ or $|\downarrow\rangle$. The probabilities of each final state are given by the Born Rule:

$$\Pr(\uparrow) = |\langle\psi|\uparrow\rangle|^2 \text{ and}$$
$$\Pr(\downarrow) = |\langle\psi|\downarrow\rangle|^2\,.$$

C. Convenient coordinates for the qubit

Our challenge is to define a set of ODEs that models this measurement process so that it can be implemented by an analog computer—that is, implemented in classical-variable coordinates. To begin, we specify how the state is stored. Equation (4) specifies the state as two complex-valued coefficients A and B. This requires 4 real-valued variables to store the same amount of information.

Removing the global phase and imposing normalization would leave the two real parameters of the familiar Bloch sphere. We go one step further and also fix the relative phase. This leaves 2 real-valued variables subject to normalization, or a single degree of freedom. First, separate the modulus and phase of the complex variables:

$$|\psi\rangle = e^{i\phi_A}|A|\,|0\rangle + e^{i\phi_B}|B|\,|1\rangle\,.$$

Next, we factor out the global phase:

$$|\psi\rangle = e^{i\phi_A}\left(|A|\,|0\rangle + e^{i(\phi_B-\phi_A)}|B|\,|1\rangle\right).$$

This global phase $\exp(i\phi_A)$ plays only a trivial role as an overall constant in the Schrödinger Equation Eq. (1) and plays no role in the Born Rule Eq. (2), since it is canceled by its complex conjugate when the modulus is taken. Therefore, we can set it to ± 1 without loss of generality, though it will be discussed more later.

In contrast, the remaining relative phase factor $\exp[i(\phi_B - \phi_A)]$ is relevant physically. However, we constrain it to ± 1 by restricting our choices of observables $\widehat{O}$

and initial conditions such that all eigenstates and initial states satisfy $\exp[i(\phi_B - \phi_A)] = \pm 1$. The result of these simplifications is that we can store the state of the qubit as:

$$|\psi\rangle = |A|\,|0\rangle \pm |B|\,|1\rangle\,.$$

This form can be drawn as the right half of a unit circle in the $|A|$-$|B|$ plane.

Next, we choose to map to an entire unit circle. We do this for two reasons:

1. This makes orthogonal states into antipodal points. For instance, $|0\rangle$ maps to $(1, 0)$ and $|1\rangle$ maps to $(-1, 0)$. This matches the up/down intuition from spin 1/2 particles, and it also ends up making the resulting dynamical system simpler.

2. It is easier to restrict a pair of voltages to the full unit circle than to half the unit circle. For a full unit circle, we only need to demand $r = 1$. For a half unit circle, we would need instead $r = 1$ and $|A| \geq 0$.

To do this map, we use the double angle trigonometric identities to define:

$$x := |A|^2 - |B|^2, \tag{7}$$
$$y := \pm 2|A||B|, \tag{8}$$

where the sign of y is chosen appropriately for the relative phase $\exp[i(\phi_B - \phi_A)] = \pm 1$. These are components of the Bloch vector: $x = \langle\widehat{\sigma}_z\rangle$ and $y = \langle\widehat{\sigma}_x\rangle$. (Note that our x coordinate is the Bloch z component.) Restricting to real amplitudes thus confines the state to the great circle of the Bloch sphere in its xz plane, and orthogonal states are antipodal on it, just as on the Bloch sphere.

The next constraint to consider is normalization. In our simplified coordinates, this is still:

$$x^2 + y^2 = 1.$$

Imposing normalization directly would reduce the state to a single real variable, the Bloch polar angle α:

$$x = \cos(\alpha) \tag{9}$$
$$y = \sin(\alpha), \tag{10}$$

with $\alpha \in [0, 2\pi)$. However, it will prove useful to have these sines and cosines available to intermediate stages in the model. (And, our circuits cannot compute them from α; see Subsection V.) Therefore, we continue to express the state in terms of x and y. We still need to impose normalization. However, this will be done dynamically. Using multipliers and amplifiers, we compute $r^2 = x^2 + y^2$, then design our equations to have a forcing term that attracts r^2 to 1.

D. Quantum evolution ODEs without measurement

Having settled on a coordinate system for our deterministic collapse model, we can begin crafting the governing differential equations. The first choice to make here is the order of our differential equations. Since the Schrödinger Equation is first order, it would be intuitive to also make our model of measurement first order. However, our integrator circuit (Fig. 6) inverts the output, so it is convenient to use a pair of them instead. Additionally, having second-order ODEs allows us to add a drag (or dissipation) term, controlled by a parameter d, which smooths out the dynamics and reduces noise that may arise in the physical circuit. With only the drag, our dynamical system so far is:

$$\begin{aligned}\dot{x} &= v_x,\\ \dot{y} &= v_y,\\ \dot{v}_x &= -dv_x,\\ \dot{v}_y &= -dv_y.\end{aligned}$$

Now, we add in a radial force that imposes normalization to the unit circle. This starts with a factor $(1 - r^2)$. Notice that this factor is zero when normalization is satisfied, positive when r is too small, and negative when r is too large. Next, this factor is applied to $\vec{r} = (x, y)$ to align the forcing term with the radial direction. Lastly, this force is scaled by a positive parameter k. Since normalization is meant to apply at all times, no matter what the rest of the equation is doing, we will choose k to be very large. With the radial force included, our dynamical system is now:

$$\dot{x} = v_x, \tag{11}$$
$$\dot{y} = v_y, \tag{12}$$
$$\dot{v}_x = kx(1 - r^2) - dv_x, \tag{13}$$
$$\dot{v}_y = ky(1 - r^2) - dv_y. \tag{14}$$

Equations (11) - (14) are sufficient to model a qubit that is not measured. However, we will add additional forcing terms to model the qubit while it is measured.

E. Measurement

To model measurement, we begin by setting the measurement axis, picking a point on the unit circle with coordinates c and s to correspond with $|\uparrow\rangle$. By our choice of coordinates, this implies $|\downarrow\rangle$ maps to $(-c, -s)$. Next, we introduce a function θ, whose role in measurement we define shortly. Now, we can write out the ODEs with measurement terms as:

$$\dot{x} = v_x, \tag{15}$$
$$\dot{y} = v_y, \tag{16}$$
$$\dot{v}_x = kx(1 - r^2) - dv_x + \theta c, \tag{17}$$
$$\dot{v}_y = ky(1 - r^2) - dv_y + \theta s. \tag{18}$$

Via θ the new terms apply a force in the (c, s) direction. If $\theta > 0$, this will push (x, y) toward (c, s). If $\theta < 0$, this will push (x, y) toward $(-c, -s)$. Once $(x, y) = \pm(c, s)$, the measurement forcing terms will compete with the radial forcing terms, but we have chosen k to be very large, so the radial terms dominate, leaving (x, y) at (or very near) $\pm(c, s)$. Now, we see that θ decides the outcome of a measurement with its sign.

F. Deterministic stochasticity

Quantum measurement is a key phenomenon that distinguishes the behaviors of classical and quantum systems. Basic classical mechanics ignores measurement, while quantum systems react substantially. To truly take on quantum dynamics our analog qubit model must be extended to encompass the system response to measurement. And, this entails augmenting the model to incorporate Born's rule that maps from the quantum wave function to the probabilities of outcomes during the measurement process.

Thus, we still must design θ to reproduce the Born Rule Eq. (2). Conceptually, starting with the Born Rule probability, subtract a hidden variable ϕ whose value the observer does not know. For a given (x, y, c, s) configuration, θ is then positive for some range of ϕ and negative for the rest. Importantly, ignorance of ϕ makes the outcome appear random. Thus, the first step is to compute the Born Rule probability for a given (x, y, c, s) configuration.

To begin, express both $\langle\psi|$ and $|\uparrow\rangle$ in the $|0\rangle, |1\rangle$ basis as $\langle\psi| = \langle 0|A^\dagger + \langle 1|B^\dagger$ and $|\uparrow\rangle = C|0\rangle + D|1\rangle$:

$$\begin{aligned} P(\uparrow) &= |\langle\psi|\uparrow\rangle|^2 \\ &= (A^\dagger C + B^\dagger D)^2 \ . \end{aligned}$$

Next, write the coefficients A and B in terms of an angle α (as in Eq. (10)) and introduce the analogous angle β to rewrite C and D:

$$P(\uparrow) = \left[\cos(\alpha/2)\cos(\beta/2) + \sin(\alpha/2)\sin(\beta/2)\right]^2 \ .$$

From here, manipulate the expression with the product to sum and half-angle trigonometric identities:

$$\begin{aligned} P(\uparrow) &= \cos^2\left(\frac{\alpha}{2} - \frac{\beta}{2}\right) \\ &= \frac{1 + \cos(\alpha - \beta)}{2} \\ &= \frac{1}{2}\left[1 + \cos(\alpha)\cos(\beta) + \sin(\alpha)\sin(\beta)\right] \ . \end{aligned}$$

Last, convert the sines and cosines of α and β back into x, y, c, and s:

$$P(\uparrow) = \frac{1}{2}\left(1 + xc + ys\right). \tag{19}$$

Our choice to keep the x, y, c, and s coordinates has paid off: We compute $P(\uparrow)$ with only addition and multiplication. That is, we know how to compute it with an analog circuit.

This expression identifies what the hidden variable must do. We take ϕ to be a number in the interval $[0, 2]$ that is fixed for the duration of a measurement but unknown to the observer. We assume that, lacking any information about it, the observer assigns it a uniform probability density over that interval:

$$p(\phi) = \begin{cases} 1/2, & 0 \le \phi \le 2 \\ 0, & \text{otherwise} \end{cases}. \tag{20}$$

This uniformity is an assumption of the model, not a consequence of it. The construction below yields Born Rule statistics only because ϕ is uniform; a nonuniform ϕ would yield different outcome frequencies (see Sec. VI C). With this, we can finally construct our function θ based on Eq. (19) and ϕ:

$$\begin{aligned} \theta(x, y, c, s, \phi) &:= 2P(\uparrow) - \phi & (21) \\ &= 1 + xc + ys - \phi. & (22) \end{aligned}$$

For a given (x, y, c, s) configuration that yields a certain $P(\uparrow)$, θ changes sign at $\phi = 2P(\uparrow)$: it is positive for ϕ in $[0, 2P(\uparrow))$ and negative for ϕ in $(2P(\uparrow), 2]$, as depicted in Fig. 1. The probability that $\theta > 0$ is therefore:

$$\int_0^{2P(\uparrow)} p(\phi)\, d\phi = P(\uparrow),$$

and the probability that $\theta < 0$ is $1 - P(\uparrow)$. In this way, the measurement forces toward (c, s) with (apparent) probability $P(\uparrow)$ and toward $(-c, -s)$ with probability $P(\downarrow) = 1 - P(\uparrow)$. With this, we have now designed every component of the measured qubit mathematical model.

The model itself is fully deterministic: Given ϕ and the initial state, the outcome of a measurement is fixed. The randomness of the Born Rule enters only through the observer's ignorance of ϕ. We return to the question of what physical degree of freedom ϕ might represent in Section VII.

The measurement dynamics has a simple geometric picture on the circle, shown in Fig. 2. For fixed ϕ, the points $\pm(c, s)$ are attractors, and the points on the circle where $\theta = 0$ (that is, where $xc + ys = \phi - 1$) are repellers. They split the circle into two basins. States with $\theta > 0$ flow to (c, s), and states with $\theta < 0$ flow to $(-c, -s)$. The hidden variable moves the boundary between the basins. So, for a given initial state, ϕ selects one of two flows: one in which (c, s) attracts the state and $(-c, -s)$ repels it, and one with the roles reversed.

The selection holds for the whole measurement: θ cannot change sign while the state collapses. To see this, note that the forces in Eqs. (15)-(18) are the drag plus the negative gradient of

$$V(x, y) = \frac{k}{4}\left(1 - r^2\right)^2 - \frac{\theta^2}{2},$$

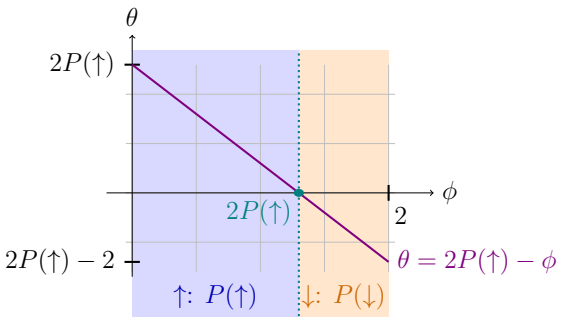

FIG. 1. Measurement outcome as a function of hidden variable ϕ: Equation (21) is positive (outcome ↑) for $\phi < 2P(\uparrow)$ and negative (outcome ↓) otherwise. For ϕ uniform on $[0, 2]$, the shaded (purple/yellow) fractions of the interval are $P(\uparrow)$ and $P(\downarrow)$, respectively.

since $\nabla\theta = (c, s)$. The energy $E = \left(v_x^2 + v_y^2\right)/2 + V$ therefore satisfies $\dot{E} = -d\left(v_x^2 + v_y^2\right) \leq 0$. A measurement starts from a normalized state at rest, where $E = -\theta_0^2/2$. Since the radial term is nonnegative, $-\theta^2/2 \leq E \leq -\theta_0^2/2$ at all later times, so $|\theta| \geq |\theta_0|$. The magnitude of θ never falls below its initial value, and its sign never changes.

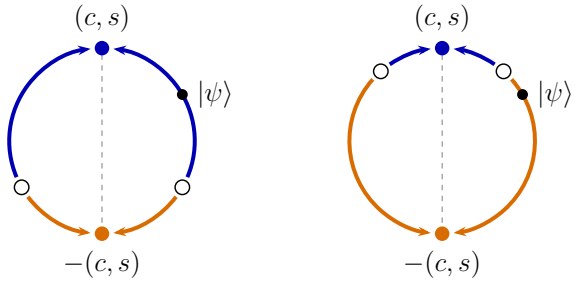

(a) $\phi = 0.5$: outcome ↑ (b) $\phi = 1.75$: outcome ↓

FIG. 2. Measurement flow on the circle of real-amplitude states, the xz great circle of the Bloch sphere, with the measurement axis (c, s) at top. Filled dots are the attractors $\pm(c, s)$, and open dots are the repellers where $\theta = 0$. States in the blue basin ($\theta > 0$) flow to (c, s), and states in the orange basin ($\theta < 0$) flow to $(-c, -s)$. The same prepared state $|\psi\rangle$, with $P(\uparrow) = 0.75$, lies in the ↑ basin for (a) $\phi = 0.5$ and in the ↓ basin for (b) $\phi = 1.75$.

G. Measured Analog Qubit

To summarize, the qubit model consists of:

1. A state recorded by coordinates (x, y).
2. A radial force, with parameter k, set very high, that forces $x^2 + y^2 \approx 1$.
3. A drag force, parameterized by d.
4. A measurement axis set by (c, s) on the unit circle.
5. A measurement force that, when turned on, forces (x, y) toward either (c, s) or $(-c, -s)$, depending on the sign of a function θ.
6. A function $\theta(x, y, c, s, \phi)$ that is positive with apparent probability $P(\uparrow)$ given by the Born Rule and negative otherwise.
7. A hidden variable $\phi \in [0, 2]$, unknown to the observer and therefore uniformly distributed from their point of view, which causes the apparent randomness. It must stay (nearly) constant while the state "collapses" to $\pm(c, s)$, so that θ does not change sign partway through a measurement.

When the qubit is not being measured, its time evolution is given by Eqs. (11)-(14). When the measurement is turned on, its time evolution is given by Eqs. (15)-(18).

Beyond being implementable, the model has the structure that Section I asked of a dynamical model of measurement. First, with the measurement force off it reduces to Schrödinger evolution: with $\widehat{H} = 0$ the state is stationary, and the radial and drag terms vanish for a normalized state at rest, acting only to restore normalization. Second, with the force on, the dynamics are nonlinear and not invertible: every initial state flows to one of two attractors, so distinct pre-measurement states end at the same post-measurement state. Third, the model respects the symmetries of the measurement. Since θ depends on the state and axis only through $xc + ys$, rotating both together leaves the dynamics unchanged, and the outcome depends only on the relative angle between them. Relabeling the outcomes, $(c, s) \to (-c, -s)$ together with $\phi \to 2 - \phi$, sends $\theta \to -\theta$ and leaves the measurement force $\theta\,(c, s)$ unchanged, so neither outcome is privileged; the uniform distribution of ϕ is invariant under this reflection.

V. ELECTRONIC ANALOG COMPUTERS

This subsection builds a repertoire of subcircuits that carry out basic mathematical operations, out of which an electronic analog computer can simulate a very wide range of physical systems. This repertoire gives an intuition for what kinds of equations are easy to simulate with an analog computer and which are not. The circuits here are standard and found in electronics textbooks [38, 39].

A. Analog Computer Functional Blocks

The most basic tool at hand is Ohm's Law, which describes how to convert a voltage to a current and scale it. If we have a resistor with resistance R and we place a voltage difference ΔV across it, a current $I = \Delta V/R$ flows from the higher voltage end to the lower voltage end. This situation is depicted in Figure 3.

With a collection of currents formed according to Ohm's Law, we add them in accordance to Kirchhoff's

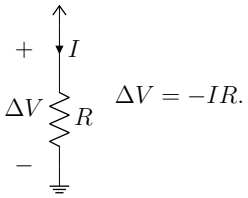

FIG. 3. Ohm's Law.

current law (KCL). KCL states that the sum of currents into a circuit node equals the sum of currents out of the node. This is depicted in Figure 4.

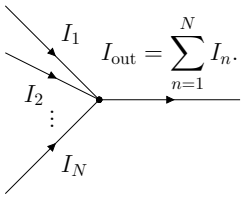

FIG. 4. Kirchhoff's current law.

So far, Ohm's Law and KCL restrict circuits to multiplication by positive scalars and addition. Negative scalar multiplication and subtraction are also needed, though. Furthermore, Ohm's Law converts voltages into currents, but turning currents back into voltages is also important.

All of these tasks are accomplished by the inverting amplifier (Figure 5). The core of this circuit is an operational amplifier (op-amp) [38, p. 635-662]. With the noninverting (+) input tied to ground ($\frac{\perp}{=}$), the amplifier equilibrates when the inverting input (−) is also at 0V and no current flows into or out of either input. This implies all current flowing through R_1 passes through the feedback resistor R_f, by KCL. By Ohm's law, this becomes:

$$\frac{V_{\text{in}} - 0\text{V}}{R_1} = \frac{0\text{V} - V_{\text{out}}}{R_f}.$$

Therefore:

$$V_{\text{out}} = -\frac{R_f}{R_1} V_{\text{in}}. \tag{23}$$

The output V_{out} acts as a voltage source, supplied by the minimum and maximum power supply voltages $V+$ and $V-$ (the voltage *rails* of the op-amp). Figure 5 depicts a single input through R_1, but this is easily extended to multiple input voltages through multiple resistors, making use of Ohm's Law and KCL. With multiple inputs $\{V_n\}$ and associated input resistances $\{R_n\}$:

$$V_{\text{out}} = -R_f \sum_{n=1}^{N} \frac{V_n}{R_n}.$$

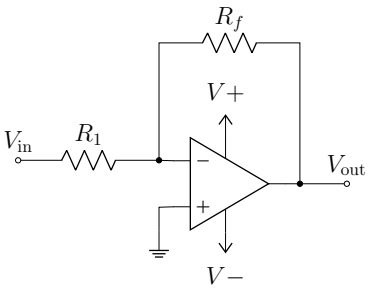

FIG. 5. Inverting amplifier circuit diagram: From Ohm's law, KCL, and the ideal op-amp assumptions, $V_{\text{out}} = -(R_f/R_1)V_{\text{in}}$.

Solving differential equations requires integrating variables that are temporal derivatives. And so, analog computers must take integrals.

The integrator circuit, depicted in Figure 6, is quite similar to the inverting amplifier, except the feedback resistor is replaced with a capacitor. The capacitor builds up charge over time, with a corresponding voltage across it such that $q = CV$. Since current is the flow rate of charge, this capacitor charge is the integral of the current flowing into it. As for the inverting amplifier, we assume that the op-amp is ideal and equilibrated. This implies the noninverting input is held at 0V and has no current flowing into it. By KCL, all current through R must flow into the capacitor. This implies:

$$\frac{V_{\text{in}} - 0\text{V}}{R} = \frac{d}{dt} C(0\text{V} - V_{\text{out}}).$$

Rearranging and integrating,

$$V_{\text{out}} = -\frac{1}{RC} \int V_{\text{in}} dt. \tag{24}$$

The product $\tau := RC$ is known as the *time constant*. It has units of seconds and sets the time scale of the integration circuit. As with the inverting amplifier, it can be easily extended to multiple inputs on multiple resistors. Picking a characteristic resistance R, this case becomes:

$$V_{\text{out}} = -\frac{1}{RC} \int \sum_n \frac{R}{R_n} V_n dt.$$

With the subcircuits so far, one can simulate any linear dynamical system, such as driven and damped simple harmonic oscillators (SHOs). However, one cannot simulate nonlinear systems, such as the Rössler or Lorenz systems, which exhibit trajectories that spread apart over time, amplifying small fluctuations and so producing perceived randomness.

To add the nonlinear terms in our nonlinear system, we need to be able to take the product of two voltages, for example. For this, we used the prefabricated AD633 integrated circuit (IC) [40]. They are wired according to

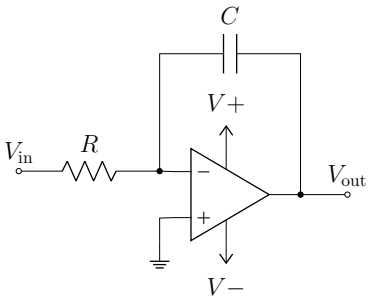

FIG. 6. Integrator circuit: Paralleling the logic of the inverting amplifier (Fig. 5), given that the voltage over a capacitor is $V_C = q/C$, $V_{\text{out}} = -(RC)^{-1}\int V_{\text{in}} dt$.

the pin-out in Figure 7. The AD633 has two differential inputs (V_1 and V_2 on pins 1 and 3), similar to the inputs on op-amps. For simplicity, we ground the inverting parts of the differential inputs (pins 2 and 4). For the output, there is an optional constant shift (pin 6), which is set to zero by grounding. The IC is supplied with external power via positive (V^+, pin 8) and negative voltage (V^-, pin 5) rails (also like an op-amp). The output, the product $V_{\text{out}} = V_1 \times V_2/10$, appears on pin 7 scaled down by a factor of 10.

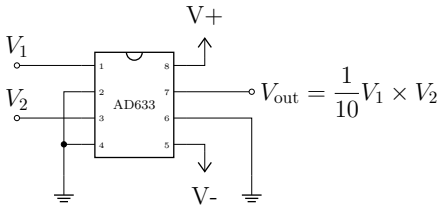

FIG. 7. AD633 multiplier IC pinout. For more details, see the datasheet [40].

To review, we now have circuits that allow us to convert between currents and voltages, scale by positive real numbers, add currents, invert currents and convert them to voltages, take integrals, and take the product of two voltages. This set of operations is enough to simulate nontrivial ODEs, but there are still some operations that are off limits. In particular, we have not discussed circuits that take square roots, exponentials, logarithms, or trigonometric functions. We could, hypothetically, approximate these with a Taylor series, using stacked AD633 multipliers for higher order terms, but this would be unnecessarily resource intensive.

There are, however, analog circuits that perform logarithms and exponentials. For example, replacing the integration capacitor with a diode in the feedback loop gives a logarithmic operation, as the diode current depends exponentially on the voltage. Similarly, replacing the input resistor with a diode gives an anti-logarithmic operation. Using these provides a much wider range of ODEs that can be simulated. These possibilities aside, we treated the list of operations above as exhaustive; this is the design constraint that shaped the qubit model of Subsection IV A.

B. Analog Implementation

With the mathematical model set and the functional blocks in hand, we can explain the design of the analog computer that implements the qubit model. A block diagram for the full computer is given in Fig. 8. The major components are:

1. Double integrators for x and y: Perform the integrals that solve the differential equations and store the current state coordinates.
2. Radial force module: Computes $1 - r^2$ and returns that to the x and y integrators.
3. Microcontroller: Initially, sets the (c, s) coordinates of the measurement axis and the hidden variable ϕ, turns the measurement force on and off (off corresponds to $c = s = 0$), and records data.
4. Interface module: Uses amplifier circuits to shift between the voltages of the microcontroller and the voltages used by it.
5. Coupling module: Computes θ and then subsequently the measurement forcing terms.

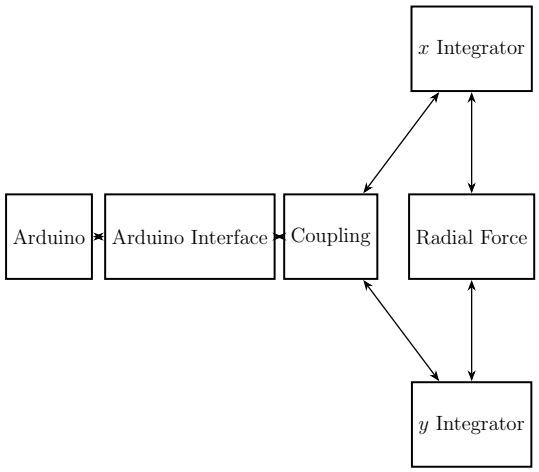

FIG. 8. Block diagram for the analog computer implementation of a qubit.

Not shown in the block diagrams is the power supply. All op-amps in the circuit are LF411s [41], and they and the AD633 multipliers run from ±15 V rails provided by a benchtop supply (labeled G in Fig. 18).

The first major subcomponents are the double integrators for x and y. As the name suggests, these take currents corresponding to the terms in $\dot{v}_{x/y}$ Eq. (17) and integrates them twice to compute x or y. The circuit diagram for x is shown in Fig. 9. The circuit for y is

identical, except it takes input from θs instead of θc and outputs y and y^2 instead of x and x^2.

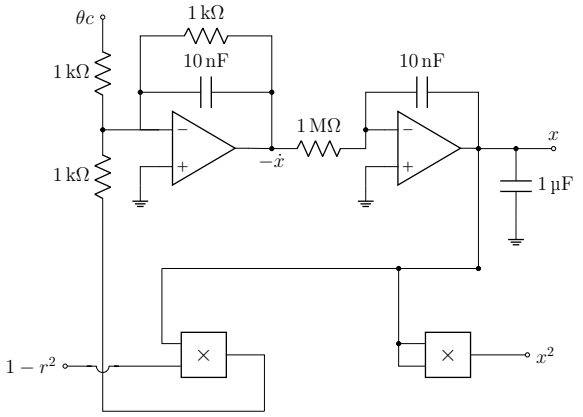

FIG. 9. Double integrator circuit: Computes x from currents corresponding to $\dot{v}_x$ by integrating twice. The first (damped) integrator outputs $-\dot{x}$; the second outputs x. The y circuit is identical, with θs, $-\dot{y}$, y, and y^2 in place of θc, $-\dot{x}$, x, and x^2. Boxes marked $\times$ are AD633 multipliers (Fig. 7), each outputting $V_1 V_2/10\,\mathrm{V}$; their power connections are omitted here and in Figs. 12 and 13.

Next is the radial force module, which computes $1-r^2$ to determine if x and y are properly positioned on the unit circle. This is depicted in Fig. 10. The inputs are the multiplier outputs $V_x^2/10\,\mathrm{V}$ and $V_y^2/10\,\mathrm{V}$, and the constant term comes from a voltage divider on the $+5\,\mathrm{V}$ rail feeding the noninverting input. With a $47\,\mathrm{k\Omega}$ over $10\,\mathrm{k\Omega}$ divider and a noninverting gain of 21, the module outputs

$$V_{\mathrm{out}} = 25\,\mathrm{V}\left[\frac{14}{19} - \left(\frac{V_x}{5\,\mathrm{V}}\right)^2 - \left(\frac{V_y}{5\,\mathrm{V}}\right)^2\right],$$

so the state settles on a circle of radius $R_{\mathrm{eq}} = \sqrt{14/19} \approx 0.858$ natural units ($\approx 4.3\,\mathrm{V}$) rather than the unit circle ($5\,\mathrm{V}$). This is a deliberate compromise. A radius of exactly $5\,\mathrm{V}$ would require a divider ratio of 3.2 (e.g., $32\,\mathrm{k\Omega}$ over $10\,\mathrm{k\Omega}$), which is not a standard off-the-shelf resistor value, so the circuit was built from standard resistors and the resulting radius is compensated in how ϕ is sampled (Subsection V C).

The coupling module is complex enough to warrant its own block diagram, depicted in Fig. 11.

As discussed in Subsection IV A, θ is the term that decides which measurement outcome is chosen, in accordance with the Born Rule with the hidden variable ϕ as the source of apparent randomness. The circuit computing θ is documented in Fig. 12.

The next subcircuits of the coupling module are the x/y coupling terms. These take θ and the measurement axis coordinates (c, s) as input, multiplies them, and computes the forcing terms θc and θs that are fed into the integrators to perform measurement on the qubit. These subcircuits are diagrammed in Fig. 13.

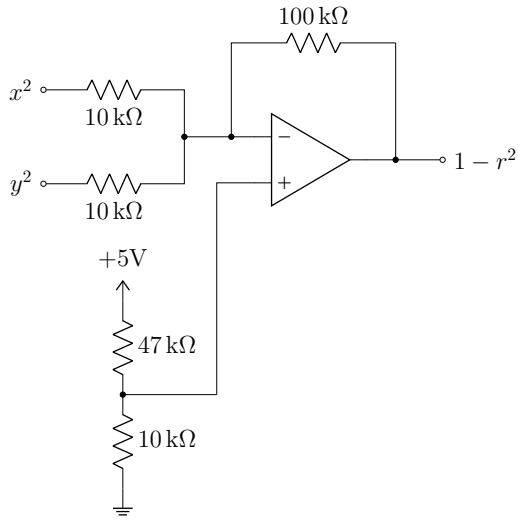

FIG. 10. Radial force module: Compute the displacement of (x, y) from the unit circle, which is taken as input to the x/y integrators to create a restoring force that keeps the state on the unit circle.

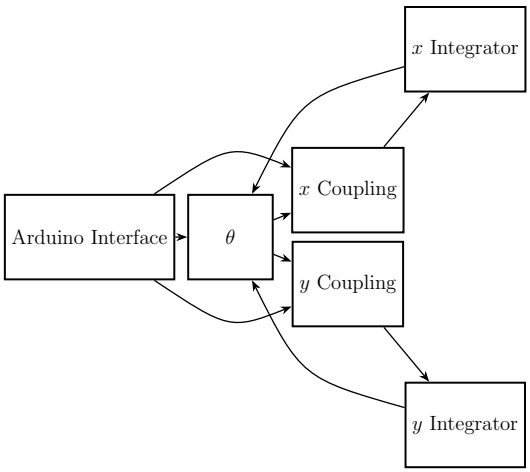

FIG. 11. Coupling module: Computes measurement forces on the qubit.

The last module is the Arduino microcontroller interface module, consisting of several amplifiers that convert between Arduino voltages (ranging from 0V to 5V) and the voltages used in the analog computer (from −5V to 5V). For c, s, and ϕ, these amplifiers draw from the PWM (pulse-width modulation) pins on the microcontroller, which mimic analog voltages by rapidly switching a digital signal on and off. To smooth these out, each PWM output feeds a second-order active low-pass filter in the Sallen-Key topology [42], which places two resistor-capacitor stages around an op-amp. A low-pass filter passes slowly varying signals (here, the intended steady voltage) and suppresses rapidly varying ones (the PWM switching). The output of a second-order filter

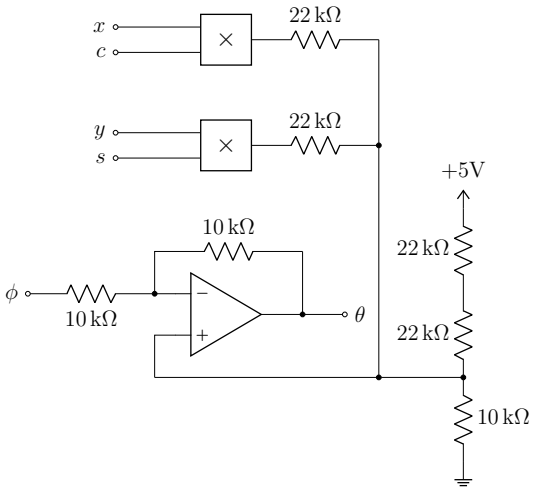

FIG. 12. Subcircuit that computes the θ term of the qubit model, which decides measurement outcomes.

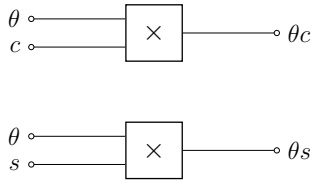

FIG. 13. Subcircuit that computes the measurement force terms θc and θs.

obeys the same equation as a driven, damped harmonic oscillator:

$$\ddot{V}_{\text{out}} + \frac{\omega_0}{Q}\dot{V}_{\text{out}} + \omega_0^2 V_{\text{out}} = K\omega_0^2 V_{\text{in}}, \tag{25}$$

so the filter is characterized by three numbers. The gain K is the ratio $V_{\text{out}}/V_{\text{in}}$ for a constant input. The natural frequency ω_0 sets where suppression begins: inputs oscillating well below ω_0 pass through (multiplied by K), while the amplitude of inputs well above ω_0 falls off as $(\omega_0/\omega)^2$. The quality factor Q is the usual measure of an oscillator's damping: $Q = 1/2$ is critically damped, and larger Q is underdamped, producing a resonant peak near ω_0. Both filters are designed for a Butterworth response, $Q = 1/\sqrt{2}$, which keeps the gain as flat as possible below ω_0 without a resonant peak [43]. For this choice, $\omega_0 = 2\pi f_{-3\,\text{dB}}$, the frequency at which the output amplitude has fallen to $1/\sqrt{2}$ of its low-frequency value. We quote suppression in decibels (dB), $20\log_{10}$ of an amplitude ratio, so that each factor of 10 in frequency above ω_0 adds 40 dB of suppression.

For the other amplifiers, the general process starts with analog voltages in the model, amplifies them to map nicely onto the $0-5$V range, then feeds the outputs to the microcontroller's analog pins for measurement and recording. These are depicted in Figs. 14 - 17.

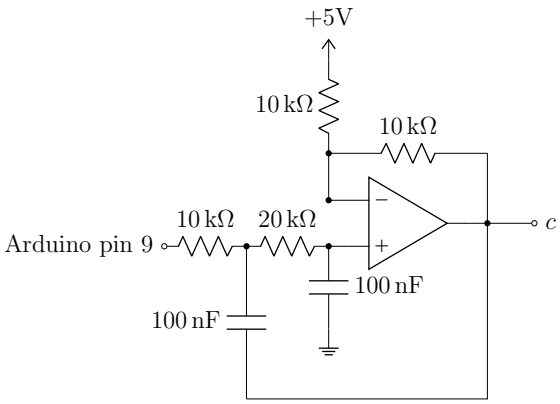

FIG. 14. Circuit that converts a PWM signal from the microcontroller (pin 9) into a stable voltage for c. The gain-2, +5V-referenced level shifter doubles as the amplifier of a second-order Sallen-Key low-pass filter. With equal capacitors and $K = 2$, $Q = \sqrt{R_1/R_2}$, so $R_2 = 2R_1$ gives a Butterworth response with $f_{-3\,\text{dB}} \approx 113\,\text{Hz}$, attenuating the 31.4 kHz PWM carrier by $\approx 98\,\text{dB}$. An identical circuit on pin 10 drives s.

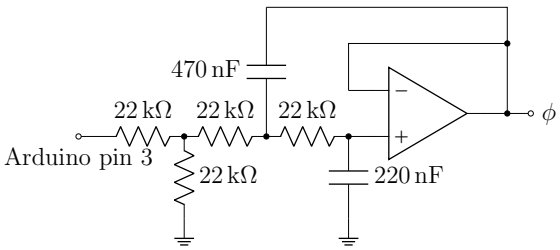

FIG. 15. Circuit that converts a PWM signal from the microcontroller (pin 3) into a stable voltage for ϕ. A 2:1 input divider (DC gain 1/2, leaving headroom at the top of the PWM range) feeds a unity-gain second-order Sallen-Key low-pass filter. Including the divider's Thévenin resistance, $Q \approx 0.72$ (near Butterworth) and $f_{-3\,\text{dB}} \approx 18\,\text{Hz}$, attenuating the $\approx 490\,\text{Hz}$ PWM carrier by $\approx 57\,\text{dB}$.

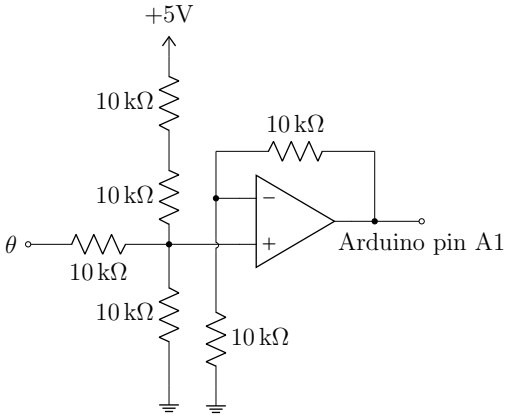

FIG. 16. Level-shifting amplifier for θ, allowing θ to be read and recorded by the microcontroller (analog pin A1). The pin voltage is $2\,\text{V} + 0.8\,V_\theta$.

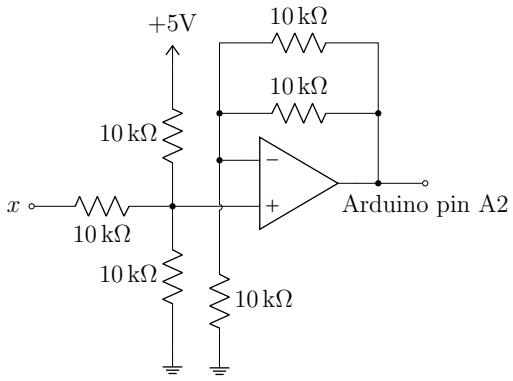

FIG. 17. Level-shifting amplifier for x, allowing it to be read and recorded by the microcontroller (analog pin A2). The pin voltage is $2.5\,\mathrm{V} + 0.5\,V_x$. A copy of this amplifier on pin A3 reads y.

C. Voltage scaling and calibration

The circuit represents the model variables x, y, c, and s with 5 V per natural unit, while θ and ϕ have their own scale of $50/47$ V per natural unit, set by the resistor ratios in the coupling module. The one departure from the ideal model, the equilibrium radius set by the radial force module, is compensated in how ϕ is chosen rather than in hardware.

As described above, the radial force module (Fig. 10) holds the state on a circle of radius $R_{\mathrm{eq}} = \sqrt{14/19} \approx 0.858$ instead of the unit circle. The measurement axis (c, s) is still set to unit length, so $xc + ys = R_{\mathrm{eq}} \cos\Delta$, where Δ is the angle between the state and the measurement axis. The θ circuit (Fig. 12), however, was designed for $r = 1$ and computes:

$$V_\theta = \frac{50}{47}\,\mathrm{V}\,(1 + xc + ys) - V_\phi,$$

so θ changes sign at $V_\phi = (50/47)(1 + R_{\mathrm{eq}} \cos\Delta)\,\mathrm{V}$. Sampling V_ϕ uniformly over $[0, 100/47]\,\mathrm{V}$, the image of $\phi \in [0, 2]$, would therefore compress the probabilities toward 1/2. Instead, V_ϕ is sampled uniformly over

$$V_\phi \in \frac{50}{47}\,[1 - R_{\mathrm{eq}},\, 1 + R_{\mathrm{eq}}]\,\mathrm{V} \approx [0.151, 1.977]\,\mathrm{V},$$

for which the fraction of ϕ values with $\theta > 0$ is $(1 + \cos\Delta)/2$, exactly the Born Rule probability Eq. (19) for a normalized state. These endpoints come from the circuit analysis, not from a fit to data.

The microcontroller is an Arduino (ATmega328P). The c and s drives use pins 9 and 10 with Timer1 reconfigured for 31.4 kHz PWM; a duty cycle D gives $V_c = (2D - 1) \times 5\,\mathrm{V}$ after the filter of Fig. 14. The measurement force is switched off by setting $c = s = 0$; because an 8-bit duty cycle cannot land exactly on 50%, the nearest code leaves $V_c = V_s \approx +20\,\mathrm{mV}$ ($c = s \approx 0.004$), half of one PWM step. The ϕ drive uses pin 3 at the default 490 Hz; after the 2:1 divider of Fig. 15, V_ϕ spans 0 to 2.5 V in steps of about 9.8 mV, giving roughly 186 distinct levels across the sampling interval. The logged value of ϕ is the quantized value actually delivered. The microcontroller holds ϕ fixed during each trial. Because we choose its value rather than leaving it unknown, we can both sample the uniform distribution of Eq. (20) efficiently (with a stratified grid) and compare each recorded outcome with the one the ideal model predicts for the same ϕ. The sampling protocol is described in Section VI. The voltages θ, x, and y are read back through the level shifters of Figs. 16 and 17 by the microcontroller's 10-bit analog-to-digital converter.

VI. RESULTS

We built the analog computer designed in Subsection V B. A picture of the computer is given in Fig. 18. The Arduino microcontroller conducts a test suite and records data that answer two questions. First, does the circuit actually implement the ODE model of Subsection IV A, to within the tolerances of its components? Second, do the empirical probabilities of the measurement outcomes obey the Born Rule?

To answer them, we perform an array of trials. In each trial the controller sets a measurement axis at a predetermined angle away from the model's current state and holds the hidden variable ϕ at a chosen value, then turns the measurement force on, lets the model equilibrate at a new state, and records where it settled. Varying both the relative angle and ϕ across trials, we compare the observed statistics to the Born Rule. Since the circuit is deterministic, we can also compare every individual outcome to the one the ideal model predicts for the same angle and ϕ.

A. Test protocol

Each trial begins with the measurement force switched on. Just before this, the controller takes the last recorded (x, y), the final reading of the preceding force-off window, and sets the new measurement axis (c, s) at the trial's relative angle Δ from it. The force stays on for about one second while (x, y) collapses to one of the two poles $\pm(c, s)$. The force is then switched off (by setting $c = s = 0$) for about one second, during which the radial force alone holds the state on the circle and the state should remain at rest. That resting state is the starting point of the next trial. This process is depicted in Fig. 19. Figure 20 shows an example of what is seen on the oscilloscope monitor while the model runs, and Fig. 21 plots the relevant signals during three consecutive trials.

The particular parameters used in testing are:

- The hidden variable takes $N = 30$ values on a midpoint grid: the sampling interval of Subsection V C

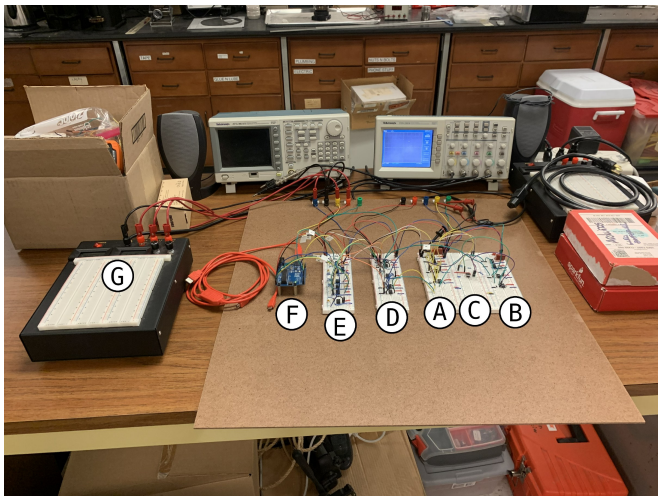

FIG. 18. Measured qubit analog computer circuit built according to Section V B's design. Major subcircuits: (A) x Integrator, (B) y Integrator, (C) Radial Force, (D) Coupling, (E) Arduino Interface, (F) Arduino, and (G) $\pm 15\,\mathrm{V}$ power supply. Test equipment in the background is not part of the circuit; the oscilloscope is used only for monitoring.

is divided into 30 equal cells and ϕ is set to the center of each. A midpoint grid is used because the fraction of its points below any threshold is an unbiased estimate of the corresponding probability; a grid that includes the endpoints biases the estimate toward 1/2.

- The relative angles Δ between the current state and the new measurement axis form a uniform grid of $m = 10$ angles from 0 to $\pi/2$ radians.
- Every combination of ϕ and Δ is run once, for $Nm = 300$ trials in a single suite. The 30 values of ϕ are visited in a shuffled order (the random seed is recorded in the log), so that any slow drift over the run is not correlated with ϕ. For each value of ϕ, the 10 angles are run in sequence. The suite opens with one force-off window, so that the first trial also starts from a recorded state.
- After ϕ is changed, the controller waits 250 ms for the ϕ filter to settle; after the axis is set, it waits 50 ms for the c and s filters to settle.
- The force-on and force-off windows each contain 20 readings of $(c, s, \theta, \phi, x, y)$ taken every $dt = 50\,\mathrm{ms}$ (54 ms in practice, including the time to transmit each reading), so a trial lasts about 2.2 s.

Both the Arduino controller code for recording data and the Python data-analysis scripts are publicly available through GitHub at `https://github.com/DelPhi-kachow/ModelQubit.git`.

We ran this suite once, recording the data through the controller's serial port; the 300 trials took 11.5 minutes. A Python script (`mqAnalysis.py`) splits the recording into trials at each rising edge of the force. For each trial it computes the realized relative angle Δ between the new axis and the state just before the force switched on, and the normalized hidden variable:

$$w = \frac{\phi - \phi_{\min}}{\phi_{\max} - \phi_{\min}} \in [0, 1],$$

where $[\phi_{\min}, \phi_{\max}]$ is the sampling interval. The outcome is $\uparrow$ ($\downarrow$) if the final state lies within 20° of (c, s) ($-(c, s)$). A final state farther than that from both poles means the collapse did not finish in time; such a trial is labeled ambiguous and counted as half $\uparrow$ and half $\downarrow$. The ideal model predicts $\uparrow$ exactly when $w < P(\uparrow) = \cos^2(\Delta/2)$.

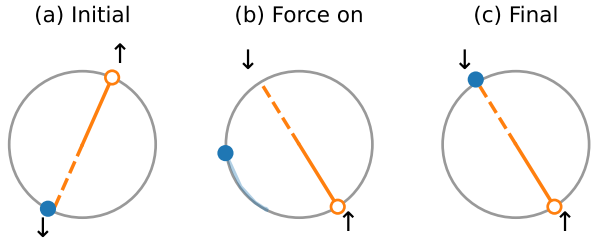

FIG. 19. Snapshots of trial 46 (relative angle $\Delta = 60°$, so $P(\uparrow) = 0.75$), in natural units: (a) The force is off and the state (blue dot) rests at the pole where the previous measurement left it, shown with that measurement's axis (orange; solid toward $\uparrow$, dashed toward $\downarrow$). (b) A new axis is set 60° away, the force is switched on, and the state begins moving; the snapshot is taken 0.11 s later, with the pale trail showing the path so far. (c) About one second later the state has equilibrated at $\downarrow$. For this value of ϕ the ideal model also predicts $\downarrow$.

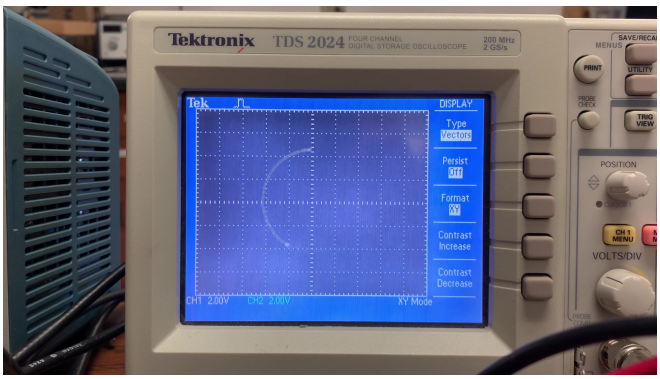

FIG. 20. Oscilloscope trace during a trial: The oscilloscope plots the (x, y) voltages at a given time. The trace persists for a time when the voltage changes, leaving a visible trail. The brightest yellow dot is the current voltage, while the fading tail depicts where the voltage was previously. In this case, we can see (x, y) is rapidly collapsing to one of the measurement equilibria.

B. Does the qubit circuit implement the model?

Before looking at probabilities, we check the circuit against the model itself. Each check compares a quantity

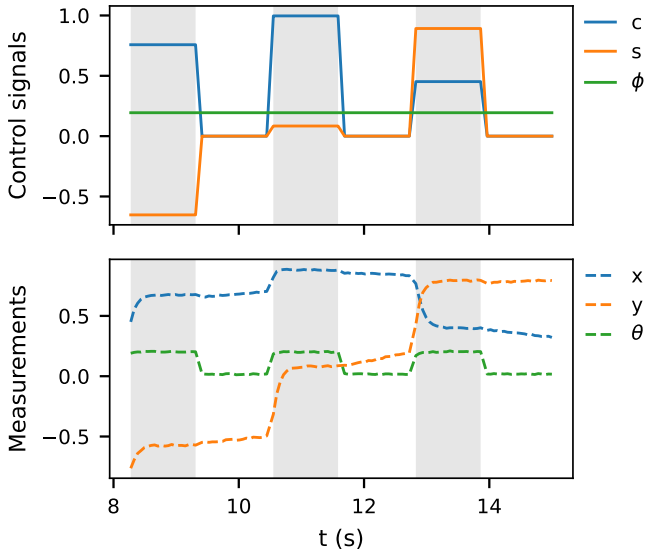

FIG. 21. Signals recorded during three consecutive trials (trials 3–5), with the force-on windows shaded: (top) The control signals. When the force is on, (c, s) is set at the trial's relative angle from the state; when it is off, both are set to zero, removing the measurement terms from the ODEs. The hidden variable ϕ is held constant, since all three trials share one of the 30 values of ϕ. (bottom) The recorded state. θ decides the outcome: if $\theta > 0$, (x, y) is driven toward (c, s), and if $\theta < 0$, toward $(-c, -s)$. Here $\theta > 0$ in all three trials and (x, y) settles near (c, s) each time. The slow change in (x, y) during the force-off windows is the drift discussed in Subsection VI D.

measured from the recording with the value designed into the circuit diagrams of Subsection V B. To judge whether a deviation is acceptable, we propagated the tolerances of the components (1% resistors, 10% capacitors, and the AD633 datasheet specifications) through the circuit diagrams by Monte Carlo (Appendix B), giving the band within which 95% of circuits built from these parts would fall. Table I summarizes the results, and Fig. 22 shows the data behind them. All voltages here are in the logged units, fractions of 5 V.

TABLE I. Circuit checks: Design values, measured values, and the central 95% band of the deviation expected from component tolerances with typical AD633 offsets (Appendix B). Errors on measured values are bootstrap standard errors over trials.

Quantity	Design	Measured	Dev.	Tolerance band
a_0	0.2128	0.2116(3)	−0.5%	±3.6%
a_u	0.2128	0.2098(2)	−1.4%	±1.8%
a_ϕ	−1	−1.0019(11)	+0.2%	±2.1%
R_{eq}	0.8584	0.8655	+0.8%	±1.0%
g (s^{-1})	50	45.7(1)	−8.6%	−9.2%, +11.0%
μ	0	+0.009(3)		−0.011, +0.013

a. θ circuit. During the force-on windows, we fit the logged θ to $\theta = a_0 + a_u u + a_\phi \phi$, where $u = xc + ys$. The design (Subsection V C) is $a_0 = a_u = 10/47$ and $a_\phi = -1$. The fit has $R^2 = 0.9998$ with an rms residual of 0.003 [Fig. 22(a)], and all three coefficients fall within their tolerance bands.

b. Radius. The settled radius is $R_{\mathrm{eq}} = 0.866$, 0.8% above the designed $\sqrt{14/19}$, again within tolerance.

c. Dynamics. The drag in the double integrators is strong enough that the velocity stages follow the forcing almost instantly, so the motion around the circle obeys a first-order law. Writing the state as $r(\cos\psi, \sin\psi)$ with unit tangent $\hat{t} = (-\sin\psi, \cos\psi)$ and measurement axis $\hat{n} = (c, s)$, gives:

$$r\dot{\psi} = g\,\theta\,(\hat{n}\cdot\hat{t}) + F_0\cdot\hat{t}.$$

The measurement gain g is set by the AD633 scale factor and the time constant of the position integrators ($1\,\mathrm{M\Omega} \times 10\,\mathrm{nF} = 10\,\mathrm{ms}$), giving a design value of $50\,\mathrm{s}^{-1}$; F_0 is a small constant force that captures drift. Fitting this law to consecutive pairs of readings gives $g = 45.7 \pm 0.1\,\mathrm{s}^{-1}$ with $R^2 = 0.992$ during the force-on windows [Fig. 22(b)]. The 8.6% shortfall is inside the tolerance band, which is dominated by the 10% tolerance of the integrator capacitors. The drift is $F_0 = (-0.048, 0.088)\,\mathrm{s}^{-1}$, about $0.1\,\mathrm{s}^{-1}$ in magnitude, compared with forcing terms of several s^{-1} while the force is on. As an end-to-end test of the dynamics, we integrate this law with the *design* gain and no drift over each force-on window, starting from the recorded state and driven by the recorded θ. The predicted final angle differs from the measured one by a median of 0.6° [Fig. 22(d)].

d. Sign rule. The model says the state collapses to $\mathrm{sign}(\theta)\,(c, s)$, with θ evaluated when the force switches on. This holds in 299 of the 300 trials. The single exception (trial 183) began with $\theta = -0.002$, essentially zero, and its collapse did not finish: it is the one ambiguous trial in the run.

e. Outcomes versus ideal model. Finally, we compare each outcome with the ideal model's prediction for the same Δ and ϕ. They agree in 296 of the 300 trials. To see why the other four disagree, define each trial's margin from the ideal threshold, $m = \cos^2(\Delta/2) - w$, so that the ideal model says ↑ exactly when $m > 0$. All four disagreements have $|m| \le 0.017$, right at the threshold [Fig. 22(c)]. A maximum-likelihood fit of $P(\uparrow) = \Phi\big((m-\mu)/\sigma_m\big)$, where Φ is the standard normal cumulative distribution function, gives a threshold bias $\mu = +0.009$ (68% interval +0.006 to +0.012) and a threshold jitter $\sigma_m = 0.006$, both in units of probability. The bias is within the band expected from the AD633 offsets. In other words, the circuit reproduces the ideal model's decisions to within one percent of the threshold.

C. Born Rule statistics

For each relative angle, the empirical probability $\hat{p}$ of collapsing to ↑ is the fraction of its 30 trials that ended

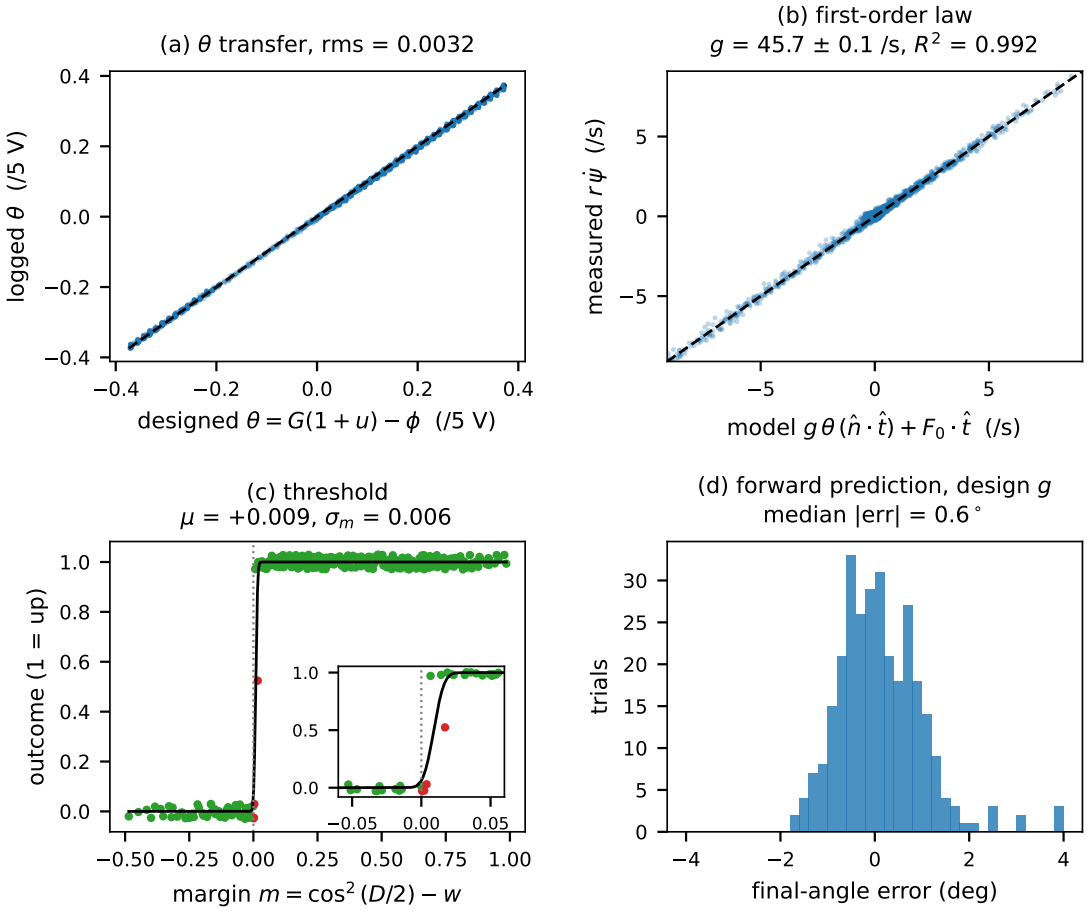

FIG. 22. Qubit circuit performance against ODE model: (a) Logged θ against the designed $\theta = G(1+u) - \phi$, with $G = 10/47$, for every force-on reading; the dashed line is equality. (b) Measured tangential velocity $r\dot{\psi}$ against the fitted first-order law. (c) Outcome (1 =↑) against the margin $m = \cos^2(\Delta/2) - w$ from the ideal threshold, with the fitted threshold curve; green points agree with the ideal model and red points do not. The inset enlarges the region near $m = 0$ (points are jittered vertically for visibility). (d) Final angle predicted by integrating the first-order law with the design gain, minus the measured final angle.

at ↑ (with the ambiguous trial counted as one half). It is compared with the Born Rule probability $\cos^2(\Delta/2)$ averaged over the realized angles of those trials. The results are plotted in Fig. 23. More details, including an animation of all 300 trials collapsing and diagnostic animations of individual trials, are available on the aforementioned GitHub repository.

The error bars come from an error model built from the data (Appendix A). It has three parts. The first is the sampling of the hidden variable: with 30 values of ϕ, each empirical probability is a 30-point estimate of an integral over ϕ, precise to about $1/(2N) \approx 0.017$. The second is the circuit's own threshold noise, taken from the fit of μ and σ_m above. The third accounts for ambiguous trials. The resulting error bars range from 0.011 to 0.022. Monte Carlo simulation of the model reproduces the spread of $\hat{p}$ to within a few percent in every bin.

Against these error bars, the empirical probabilities agree with the Born Rule with $\chi^2 = 7.2$ for 10 degrees of freedom ($p = 0.71$), and the rms difference between $\hat{p}$ and the Born Rule is 0.013. For comparison, a perfect circuit run with exactly the same 30 values of ϕ would differ from the Born Rule by 0.010 rms, so most of the remaining difference comes from the finite sampling of ϕ rather than from the circuit. We conclude that the analog qubit recreates Born Rule statistics to within about 0.02 in probability.

Since the circuit is deterministic, a departure from the Born Rule enters only through a few identifiable routes, each of which the checks above constrain. A bias μ in the decision threshold shifts every probability by about μ; the fitted $\mu = +0.009$ is below the size of the error bars. A distribution of ϕ that is not uniform over its sampling interval, or a θ circuit that responds to ϕ nonlinearly, would distort $P(\uparrow)$ into a different function of the angle; the ϕ values here are set on a uniform grid and read back, and the fitted θ depends linearly on ϕ with a coefficient within 0.2% of design. Finally, a ϕ that changed during a collapse could flip the sign of θ partway through; the sign rule holds in 299 of 300 trials. None of these routes is detectable in the present data. Conversely, introducing them on purpose, for example by drawing ϕ from

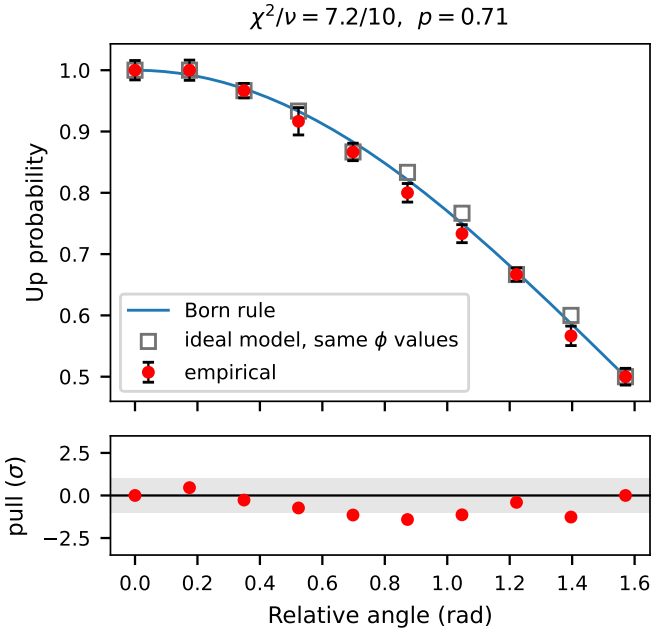

FIG. 23. Empirical probability of collapsing to ↑ against the relative angle between the state and the measurement axis: (top) Measured probabilities (red, with error bars from the error model of Appendix A) compared with the Born Rule (blue line) and with what a perfect circuit gives for exactly the same values of ϕ (open squares). (bottom) Pull, $(\hat{p}-P_{\text{Born}})/\sigma$, for each relative angle; the shaded band is $\pm 1\sigma$.

a nonuniform distribution, would produce controlled departures from the Born Rule, which we leave to future work.

D. Remaining limitations

An analog circuit implementing a measured qubit brings with it its own limitations. Let's address four of these:

1. *Resolution of the hidden variable.* With 30 values of ϕ, the empirical probabilities cannot resolve the Born Rule more finely than about 0.017. The number of values is limited by run time: the circuit's time scale was chosen so that a trial takes a couple of seconds and can be followed on an oscilloscope in real time, both for troubleshooting and as a visual demonstration of the computation. The resolution of the PWM drive for ϕ (about 186 levels across the sampling interval) would allow a somewhat denser grid.

   In practice, one swaps out resistors and capacitors in the double integrators to run the experiment much faster. The LF411 op-amps [41] used in our analog computer have a slew rate high enough to handle signals into the audio range. The upshot is that we can, easily, run the model 100 times faster by swapping out the 1 MΩ resistors in the double integrators with 10 kΩ resistors.
2. *Drift.* With the force off, the state is not perfectly at rest; it drifts at about $0.1\,\text{s}^{-1}$ (the fitted F_0), which can be seen in the force-off windows of Fig. 21. Since each trial's relative angle is measured from the state just before the force switches on, the drift does not bias the comparison with the Born Rule. And, while the force is on, it is small compared with the measurement forcing. The drift likely arises from small asymmetries between the x and y channels, such as the 10% tolerance of the integrator capacitors and the multiplier offsets, which are amplified by the large radial force constant k. Weakening the radial force would reduce the drift, at the expense of letting the state stretch off the circle.
3. *Incomplete collapse.* When θ is very close to zero, the measurement force is weak and the collapse may not finish within the force-on window. This happened once in 300 trials (trial 183), which was counted as half ↑ and half ↓ and contributes to the error bar of its bin.
4. *Offsets.* The threshold bias $\mu = +0.009$ and the 8.6% shortfall in the measurement gain are both within the tolerances of the parts. The gain affects only how fast the state collapses, not where it goes. The bias shifts every threshold by about one percent and is the largest systematic effect on the outcomes; trimming the AD633 offsets would reduce it.

VII. DISCUSSION

We demonstrated how to design a deterministic dynamical system that models measurement in a single qubit. Our electronic analog computer implementation confirmed that this model recreates the statistics of the Born rule to within about 0.02 in probability and that the circuit reproduces the ideal model's individual outcomes to within one percent of the decision threshold. In this way, the implementation illustrated the potential of deterministic collapse theories, which explain measurement with a deterministic dynamical system that modifies the Schrödinger equation with nonlinear terms. Beyond the theoretical implications, the analog implementation itself demonstrates the ability of deterministic dynamical systems to replicate key aspects of the behavior of quantum systems. More exploration is needed to probe how practical measured analog qubits will be for our eventual target of 100s or 1000s of them coupled on VLSI substrates.

Before touching on the physical implications, we should discuss the limitations of our model. Although the model has the structure required of a dynamical model of measurement (Subsection IV G), the particular equations are ad hoc, and we certainly do not offer them verbatim as a final theory of measurement. In particular, we recognize that the model's θ term, defined in Eq. (21) to

decide the measurement outcome via its sign, only makes sense for a system with two distinct measurement outcomes (a qubit). Furthermore, the construction of Eqs. (15) - (18) is constrained to be easily implemented on an analog computer, using only sums, differences, and products in the equations of motion. This constraint is not motivated physically, but chosen for ease of construction. There are no doubt similar models that also recreate Born rule statistics but use terms that would not be easily implemented as an analog circuit. However, these alternative constructions would still fall under the umbrella of "deterministic collapse theories".

The particular equations of motion aside, the truly salient feature of our model is that it is a deterministic nonlinear system that reduces to Schrödinger evolution when a measurement is not happening, but creates Born-rule statistics when a measurement occurs. Measurement is produced by nonlinear time evolution, which is interpreted as a superposition-violating Hamiltonian. This interpretation is tautologically correct if the Hamiltonian is defined as the generator of time evolution rather than a physical notion of energy. Intuitively, this makes sense, as a measurement must be able to distinguish between an arbitrary superposition of basis states and a pure eigenstate of the measurement. All deterministic dynamical collapse theories posit a continuous interpolation between unitary (Schrödinger) and nonunitary (measurement) dynamics. This aspect is shared with the continuous spontaneous localization theory [23] and the Diósi-Penrose theory [24], though deterministic collapse differs from these by not positing a source of intrinsically random noise.

The model's state is classical. An agent with direct access to the circuit's voltages could read out (x, y), or copy it, as anyone probing the circuit does. The model is meant to describe the qubit as seen by an observer whose only access to it is through measurement: switching on the measurement force and recording the outcome. With that restriction, the model respects the single-qubit counterpart of no-cloning, that nonorthogonal states cannot be reliably distinguished from one measurement. The outcome depends on the state only through $P(\uparrow)$, compared against the unresolved ϕ, so one measurement reveals no more about the state than a projective measurement in standard quantum mechanics. This is not automatic. A measurement force that ignored ϕ, such as $\theta = xc + ys$, would distinguish nonorthogonal states deterministically. Requiring the outcome to depend on the state only through its Born probabilities is therefore a real constraint on the allowed measurement dynamics. In our model, it stands in for the protection that linearity provides in standard quantum mechanics.

Our model and experiment say nothing about where the hidden variable ϕ comes from; they require only that it be uniformly distributed from the observer's point of view and that it hold still while a measurement completes. By way of looking to future efforts, let's discuss various options to these constraints.

One natural way to meet both requirements is for ϕ to be a fast, deterministic oscillation whose phase the observer cannot resolve. A triangle wave spanning $[0, 2]$, for instance, spends equal time at every value, so an observer who triggers a measurement at an imprecisely known time sees a uniformly distributed ϕ, provided the period is long compared with the collapse time but short compared with the observer's timing uncertainty. It is then suggestive to imagine that this oscillation corresponds to the global phase of the qubit, which would oscillate very fast, generating apparent randomness. For instance, oscillation due to an energy difference on the order of 1 eV would be on the order of 200 THz. If the measurement apparatus were treated as part of the system under study, we would instead be tempted to interpret ϕ as a relative phase between the qubit and the measurement apparatus. One motivation to expect this is that nonlinear terms in a Hamiltonian with respect to $|\psi\rangle = A|0\rangle + B|1\rangle$, proportional to A^n or B^n, would oscillate faster with respect to the phase of $|\psi\rangle$ than linear terms (a linear combination of A and B). Phase as the hidden variable of dynamical collapse becomes testable when oscillations occur at observable time scales.

Dynamical collapse theories are hidden-variable theories, so Bell's theorem (Sec. I) applies to them. Two points keep it from ruling out our model. First, Bell's theorem constrains only correlations between two or more systems. A single qubit, which is all our circuit models, admits a deterministic hidden-variable description; Bell himself constructed one for a spin-1/2 particle [1]. The theorem applies only once the model is extended to entangled pairs. Second, in such an extension the collapse dynamics of each qubit would depend on the joint state, making dynamical collapse a *nonlocal* hidden-variable theory, which is not bound by Bell's inequality. (The other escape route, abandoning Bell's assumption of statistical independence [44], is not needed here.) Standard quantum mechanics is nonlocal in the same way; observers in different reference frames will have the same measurement outcomes, but they will disagree about the causal ordering of states and collapses.

This curt answer to entanglement is not enough to prove consistency with causality; more investigation is still needed. In particular, we are developing an explicit dynamical collapse model of a Bell test to explore this. Dynamical collapse adds new meaning to the state of a system, because it is now also defined (and continuously evolving) during a measurement. It is desirable to have an account of state trajectories in different reference frames and a transformation rule between them. More work is needed to definitively show that dynamical collapse is consistent with causality. However, it is safe to say that Bell's Theorem does not rule out dynamical collapse theories from the outset.

This model is similar in spirit to that of Weinberg [26], who used observables that are nonlinear functions of the state. Gisin and Polchinski showed that Weinberg's nonlinear dynamics permits superluminal signal-

ing [27, 28, 45]. Linearity is the standard guarantee against this. By the no-cloning argument of Sec. II B, linear dynamics cannot copy an unknown state, and so cannot be used to signal through entanglement [6]. Linearity is sufficient for no-signaling, however, not necessary. Gisin's argument assumes that the nonlinear evolution depends only on the quantum state. A distant party's choice of measurement then prepares different ensembles of pure states with the same density matrix, and the nonlinear evolution tells them apart. Our class of models does not satisfy that assumption: its dynamics also depend on the hidden variable ϕ, which standard quantum mechanics does not represent. (Above, we speculated that ϕ may be a global phase.)

Pilot-wave theory shows that such an escape is possible in principle. Its guidance equation is nonlinear and nonlocal, yet it permits no signaling as long as particle positions are Born-distributed, a condition known as quantum equilibrium. Valentini showed that this holds in any deterministic hidden-variable theory: signaling is impossible in equilibrium and generically possible outside it [46]. Our model is such a theory, and the requirement that ϕ be uniformly distributed from the observer's point of view plays the role of equilibrium. We therefore expect no-signaling in a multi-qubit extension of the model, if it can be achieved, to rest on that requirement. Because cloning would itself permit signaling [6], establishing no-signaling for entangled qubits would also settle whether the model admits cloning. This is a central question for the dynamical-collapse Bell test described above.

Bielińska, Eckstein, and Horodecki recently reexamined Gisin's no-go theorem in light of later developments, clarifying which of its assumptions a nonlinear model must evade to avoid superluminal signaling. They showed that such nonlinear dynamics is generically chaotic [47]. Dependence on a variable hidden from standard quantum mechanics is one candidate route through these loopholes, though more work is needed to be certain.

The literature on weak measurements provides further insight into how deterministic collapse models ought to be refined. Patel and Kumar show that imposing continuous satisfaction of the Born rule is sufficient for satisfying relativity, and they give stochastic models of time evolution that satisfy this [48]. On the experimental side, Murch et al. use a state tomography technique to "watch" the state of a superconducting qubit embedded in a microwave cavity as it collapses under weak measurement [49]. These observations show the state undergoing what appears to be a random walk towards an eigenstate of the measurement. Qualitatively, this means that theoretical models of measurement should not give ballistic trajectories; they should model the noise. This poses a challenge to deterministic collapse models, which will likely require modeling nonlinear coupling of the state to the environment in addition to between the state and the measurement device.

In addition to harmonizing dynamical collapse with causality and modeling the noisiness of weak measurement experiments, there are several other paths to follow on the theory side:

1. A dynamical collapse model that accounts for more than two discrete states.
2. A dynamical collapse model for a continuous basis, such as with position or momentum.
3. Investigation into other hidden variables as sources of sensitive dependence on initial conditions. We posited global phase (or relative phase between object and measurement device). Besides variables that are completely hidden to quantum theory, there are other variables that are only "slightly hidden", particularly states in the measurement device and states in the environment, which are still traced out when constructing the system's reduced density matrix.
4. A dynamical collapse model in QFT, which would likely come out as an extension of causality, as in QFT.
5. Devising concrete experimental tests for intermediate regimes between unitary evolution and measurement.
6. Devising concrete experimental tests for particular hidden variable dependence.
7. Measurement of two entangled qubits. This requires designing measurement forces that act on a joint state, and it is also the setting for an explicit dynamical-collapse model of a Bell test.
8. Chaos. The present model collapses onto fixed points. Whether the framework can produce chaotic dynamics, and what that would mean for the corresponding quantum system, is open; nonlinear quantum dynamics is known to be generically chaotic [47].
9. Robustness to noise. Adding Langevin noise to the equations of motion, or to the circuit, and measuring how the Born-rule frequencies degrade would connect deterministic collapse to the stochastic collapse theories and to the noisy trajectories seen in weak measurement.
10. A geometric formulation. Our model restricts the qubit to real amplitudes, a great circle of the Bloch sphere. Geometric quantum mechanics describes states as points and distributions on complex projective space [50], and would be a natural language for extending deterministic collapse to the full state space.
11. Speed limits: Bounding how fast collapse can proceed. Our model is a dissipative deterministic system whose collapse rate is set by the measurement gain and drag, making it a natural test case for recent speed limits on deterministic dynamical systems, which bound the rate of change of observables using a classical analog of the density matrix and Fisher information on the tangent-space dynamics [51, 52].

In view of these, our construction of an analog qubit appears to open up a number of empirical and theoretical challenges.

VIII. CONCLUSION

Fundamental physics aside, these results may have applications in the realm of computer engineering. We demonstrated that a single classical dynamical system can reproduce the behavior of a measured qubit: The same equations describe both nonmeasurement evolution and continuous collapse when the measurement coupling is turned on, and the outcomes follow Born-rule statistics. This is less than full quantum behavior. The model's state is classical information, and whether the dynamics can be extended to entangled qubits without permitting cloning or signaling remains open (Sec. VII). As mentioned in the introduction, such systems could be useful for efficiently simulating quantum algorithms on classical systems. However, we have not demonstrated here that such analog computers can easily construct high-dimensional Hilbert spaces, which is the same problem encountered by other attempts to create (nonmeasurement) analogs to quantum computing [34, 35].

To understand the scalability problem more deeply, we need to contrast the amount of hardware needed for a quantum computer against our current approach to constructing an analog simulation. In a real quantum computer, one constructs a number N of qubits, then runs those qubits through a quantum circuit, possibly taking measurements throughout the process. The state space of these N qubits is 2^N-dimensional, with each dimension being a complex number. Our analog emulation approach uses a separate voltage to model each real-valued parameter. It takes two real variables, x and y, to model each complex variable of the form $z = x + iy$. Thus, our current approach to analog simulation requires 2^{N+1} subcircuits to model the same N qubits. This results in an exponential growth in the number of component parts, making simulation of large quantum computers infeasible.

This blow-up is depicted in Fig. 24. Suppose that, by some technological miracle, we could construct a circuit that evolved a mole of real variables ($\approx 6 \times 10^{23}$). Such a device could only simulate 77 qubits. A more reasonable achievement would be modeling a billion parameters, which allows emulation of 19 qubits. This is not enough to achieve the much-renowned "quantum supremacy" on an analog computer. Then again the path to achieving this would likely be instructive for resource scaling.

Solving the scalability problem would require designing a classical analog to the tensor product, somehow allowing the implicit creation of new degrees of freedom through interactions between subsystems (like entanglement), rather than having to explicitly construct all degrees of freedom beforehand.

Intuition that such systems may exist comes from entropy creation and bifurcations in dynamical systems theory. For instance, the number bits needed to accurately predict the chaotic Baker's Map grows with the number of time steps [53, p. 464]. Each new bit can be thought of as a new (binary) variable, though the only physical form of storage is a single real number undergoing nonlinear time evolution.

Additionally, it is notable that probability distributions of coupled variables already have a tensor product structure, which may prove a fruitful direction of inquiry. At the macroscopic level, something like a fluid can be treated this way, as a time-evolving ensemble. However, approaches like these are likely to face a roadblock in that the continuum hypothesis eventually breaks down at some level of granularity, and a material substance has only a list of continuous variables that grow linearly with the number of particles, unlike quantum mechanics. Such limitations are discussed in [54, 55].

A scalable classical analog would also open a new class of benchmarks. In many-qubit circuits, interleaving measurements with unitary gates drives a transition from extensive (volume-law) to bounded (area-law) entanglement as the measurement rate increases [56], and such measurement-induced phase transitions have now been observed on quantum hardware [57]. Because measurement is precisely the ingredient our model adds to earlier analog simulators, these transitions would be a natural test for an analog emulator of many measured qubits.

In summary, this analog simulation of measuring a single qubit motivates a broader research program with two distinct high-payoff directions. For the foundations of quantum mechanics, this work revives interest in nonlinear dynamical systems as a framework for attacking the measurement problem, though causality problems remain a significant obstacle. On the engineering side, classical analog emulation of quantum systems hints at the possibility of efficiently simulating quantum algorithms without quantum hardware, though the scalability problem is as yet unsolved and would require a genuinely novel classical analog of the tensor product to overcome. Either of these directions, if successful, would have profound implications; this program gains resilience from the fact that failure in one need not preclude success in the other.

ACKNOWLEDGMENTS

We thank Fabio Anza, Jinghao Lyu, Jason R. Green, and Komal Sah for helpful comments on an earlier draft. This material is based on work supported by, or in part by, the Art and Science Laboratory.

Appendix A: Empirical probability errors

This appendix derives the error bars of Fig. 23. They represent the spread of the empirical probabilities expected if the same circuit were run again with the same

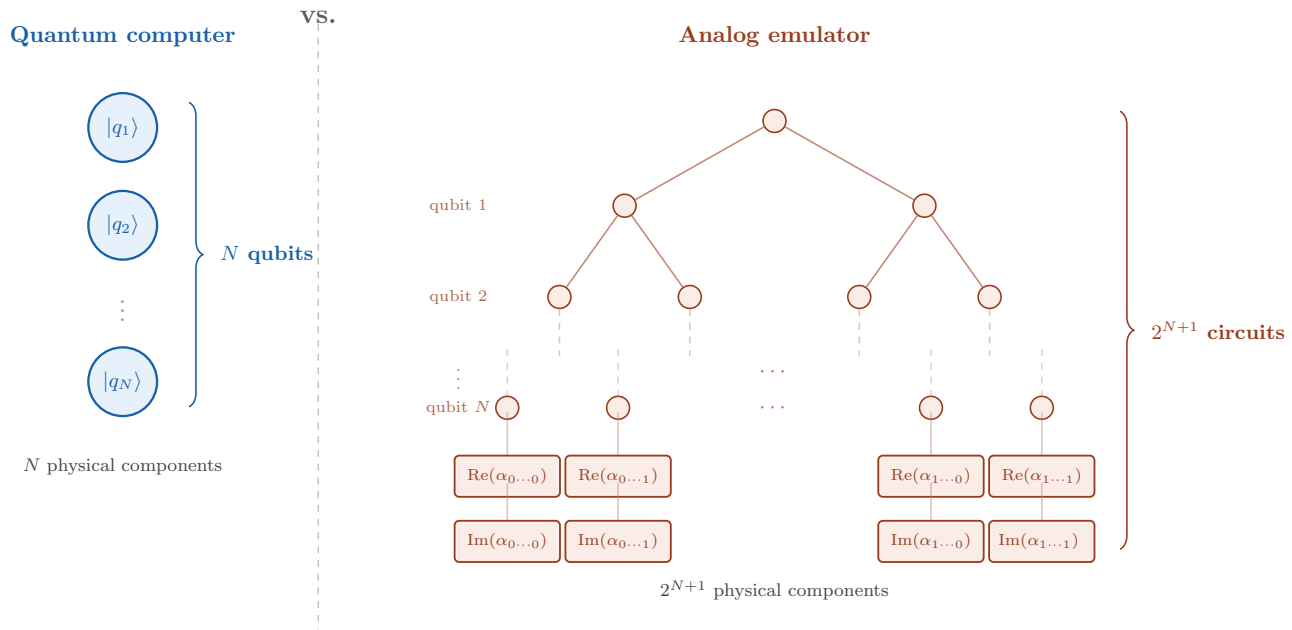

FIG. 24. Exponential blow-up of components needed to emulate N qubits using our current approach.

protocol.

Trial i has realized relative angle Δ_i, normalized hidden variable $w_i \in [0,1]$, and Born probability $P_i = \cos^2(\Delta_i/2)$. The ideal model gives ↑ exactly when the margin $m_i = P_i - w_i$ is positive. For the bin of relative angle j, containing $n_j = 30$ trials of which $n_{\mathrm{amb},j}$ are ambiguous, the empirical probability is:

$$\hat{p}_j = \frac{n_{\uparrow,j} + \frac{1}{2} n_{\mathrm{amb},j}}{n_j},$$

and it is compared with P_j, the mean of P_i over the bin. Using the mean over the realized angles means that any difference between the commanded and realized angles is accounted for in P_j rather than added to the error bar.

a. Device threshold noise. A real circuit does not switch exactly at $m = 0$. We model each outcome as ↑ with probability $\Phi\big((m_i - \mu)/\sigma_m\big)$, where Φ is the standard normal cumulative distribution function, μ is the circuit's threshold bias, and σ_m its threshold jitter, both in units of probability. The parameters are fit by maximum likelihood over all 300 trials, giving $\mu = +0.009$ and $\sigma_m = 0.006$ (Subsection VI B).

b. Hidden-variable sampling. The hidden variable takes only $N = 30$ values, so $\hat{p}_j$ is a 30-point quadrature of a step function of w rather than an exact integral. To model the resulting uncertainty, we treat each value of ϕ as a single uniform draw $w_c + U$ from its grid cell of width $h = 1/N$, where w_c is the cell center and U is uniform on $[-h/2, h/2]$. (A repeated suite would reuse the same values of ϕ, so it would share U and add no new samples of the hidden variable.) Given U, trial i in cell c is ↑ with probability:

$$p_i(U) = \Phi\left(\frac{P_i - w_c - U - \mu}{\sigma_m}\right).$$

c. Combining the two. By the law of total variance, the variance of the number of ↑ outcomes in each cell splits into a part from the hidden variable and a part from the circuit. Summing over the cells c in bin j,

$$\sigma^2_{\mathrm{HV},j} = \frac{1}{n_j^2} \sum_c \mathrm{Var}_U\Big[\sum_{i\in c} p_i(U)\Big],$$
$$\sigma^2_{\mathrm{dev},j} = \frac{1}{n_j^2} \sum_c \mathrm{E}_U\Big[\sum_{i\in c} p_i(U)\big(1 - p_i(U)\big)\Big],$$

where the sums over i run over the trials of bin j in cell c. Each ambiguous trial, counted as one half, adds $\sigma^2_{\mathrm{amb},j} = 0.25\, n_{\mathrm{amb},j}/n_j^2$. The error bar is:

$$\sigma_j^2 = \sigma^2_{\mathrm{HV},j} + \sigma^2_{\mathrm{dev},j} + \sigma^2_{\mathrm{amb},j},$$

with a floor of 0.002. The floor matters only where the grid of ϕ is symmetric about the threshold, as at $\Delta = 90°$, where the other terms nearly vanish. For this run σ_{HV} and σ_{dev} are each about 0.01, the one ambiguous trial adds 0.017 to its bin, and the combined error bars range from 0.011 to 0.022. A Monte Carlo simulation of the model reproduces the spread of $\hat{p}_j$ to within a few percent in every bin.

d. Bias of the grid. The same framework gives the expected bias of $\hat{p}_j$ for a perfect circuit, $\mathrm{E}_U[\hat{p}_j] - P_j$ with $\sigma_m \to 0$ and $\mu = 0$. For a grid that includes the endpoints

of the sampling interval, this bias pulls the estimate toward 1/2 by up to about $1/(2N)$. For the midpoint grid used here it is negligible: the values computed for this run are at most 0.003 in magnitude.

Appendix B: Component-tolerance Monte Carlo

The tolerance bands in Table I come from a Monte Carlo simulation (`toleranceMC.py` in the GitHub repository) that propagates component tolerances through the circuit diagrams of Subsection V B to the same quantities the analysis measures, in the same logged units.

Each of 40,000 simulated circuits draws every resistor uniformly within ±1% of its nominal value, every capacitor within ±10%, and each AD633 scale factor within ±0.25%. Each AD633 also receives output and input offsets, drawn uniformly within the datasheet limits [40]. Two scenarios are run: typical offsets (±5 mV at the output and inputs) and maximum offsets (±50 mV at the output, ±30 mV at the inputs). All +5 V references, including the Arduino's ADC reference, are treated as a single rail at its nominal value.

For each simulated circuit, the simulation computes the following, using the same conversions from pin voltages to logged values as the firmware:

- The θ coefficients a_0, a_u, and a_ϕ, by evaluating the θ circuit (including the drive and readout stages) over a grid of states, axes, and values of ϕ, and fitting the same linear model used on the data.
- The equilibrium radius, by solving for the voltage at which the radial force vanishes in each channel and averaging the two channels.
- The measurement gain g, from the small-signal gain of the chain from θ through the θc multiplier and the velocity and position stages to the logged x.
- The threshold bias μ, from the value of ϕ at which the simulated θ changes sign at each of the 10 relative angles, compared with the ideal threshold $\cos^2(\Delta/2)$.

The band for each quantity is the central 95% interval of its deviation from design. Table I lists the typical-offset bands; with maximum offsets they widen to −4.8% to +4.9% for a_0, ±2.4% for the radius, and −0.024 to +0.030 for μ, while the other bands are essentially unchanged. The band for g is dominated by the capacitors of the position integrators. The supply rail is not included: the slope a_u and the gain g scale in proportion to it, and the radius scales as its inverse square root, so a rail a few percent from 5 V would shift these quantities by a comparable amount.

[1] J. S. Bell, On the problem of hidden variables in quantum mechanics, Reviews of Modern Physics **38**, 447–452 (1966).

[2] D. Bohm and J. Bub, A proposed solution of the measurement problem in quantum mechanics by a hidden variable theory, Reviews of Modern Physics **38**, 453 (1966).

[3] N. Zettili, *Quantum Mechanics*, 2nd ed. (Wiley-Blackwell, Hoboken, NJ, 2009).

[4] A. Touil, F. Anza, S. Deffner, and J. P. Crutchfield, Branching states as the emergent structure of a quantum universe, Quantum **8**, 1494 (2024).

[5] W. K. Wootters and W. H. Zurek, A single quantum cannot be cloned, Nature **299**, 802 (1982).

[6] D. Dieks, Communication by EPR devices, Phys. Lett. A **92**, 271 (1982).

[7] M. A. Nielsen and I. L. Chuang, *Quantum Computation and Quantum Information*, 10th ed. (Cambridge University Press, Cambridge, 2010).

[8] M. Schlosshauer, Decoherence, the measurement problem, and interpretations of quantum mechanics, Reviews of Modern Physics **76**, 1267–1305 (2005).

[9] E. Joos and H. D. Zeh, The emergence of classical properties through interaction with the environment, Zeitschrift für Physik B Condensed Matter **59**, 223–243 (1985).

[10] W. H. Zurek, Decoherence, einselection, and the quantum origins of the classical, Reviews of Modern Physics **75**, 715–775 (2003).

[11] W. H. Zurek, Quantum origin of quantum jumps: Breaking of unitary symmetry induced by information transfer in the transition from quantum to classical, Physical Review A **76**, 10.1103/physreva.76.052110 (2007).

[12] W. H. Zurek, Quantum darwinism, Nature Physics **5**, 181–188 (2009).

[13] A. Touil, B. Yan, D. Girolami, S. Deffner, and W. H. Zurek, Eavesdropping on the decohering environment: Quantum darwinism, amplification, and the origin of objective classical reality, Physical Review Letters **128**, 10.1103/physrevlett.128.010401 (2022).

[14] L. de Broglie, La nouvelle dynamique des quanta, in *Électrons et Photons: Rapports et Discussions du Cinquiéme Conseil de Physique* (Brussels, Belgium, 1928).

[15] A. Valentini, The trouble with pilot-wave theory: a critical evaluation, in *Guiding Waves in Quantum Mechanics: One Hundred Years of de Broglie-Bohm Pilot-Wave Theory* (Oxford University Press, 2025).

[16] J. S. Bell, On the einstein podolsky rosen paradox, Physics Physique Fizika **1**, 195 (1964).

[17] J. F. Clauser, M. A. Horne, A. Shimony, and R. A. Holt, Proposed experiment to test local hidden-variable theories, Phys. Rev. Lett. **23**, 880 (1969).

[18] B. Hensen, H. Bernien, A. E. Dréau, A. Reiserer, N. Kalb, M. S. Blok, J. Ruitenberg, R. F. L. Vermeulen, R. N. Schouten, C. Abellán, W. Amaya, V. Pruneri, M. W. Mitchell, M. Markham, D. J. Twitchen, D. Elkouss, S. Wehner, T. H. Taminiau, and R. Hanson, Loophole-free bell inequality violation using electron spins separated by 1.3 kilometres, Nature **526**, 682–686 (2015).

[19] M. Giustina, M. A. Versteegh, S. Wengerowsky, J. Handsteiner, A. Hochrainer, K. Phelan, F. Steinlechner, J. Kofler, J.-Å. Larsson, C. Abellán, W. Amaya,

V. Pruneri, M. W. Mitchell, J. Beyer, T. Gerrits, A. E. Lita, L. K. Shalm, S. W. Nam, T. Scheidl, R. Ursin, B. Wittmann, and A. Zeilinger, Significant-loophole-free test of bell's theorem with entangled photons, Physical Review Letters **115**, 10.1103/physrevlett.115.250401 (2015).

[20] L. K. Shalm, E. Meyer-Scott, B. G. Christensen, P. Bierhorst, M. A. Wayne, M. J. Stevens, T. Gerrits, S. Glancy, D. R. Hamel, M. S. Allman, K. J. Coakley, S. D. Dyer, C. Hodge, A. E. Lita, V. B. Verma, C. Lambrocco, E. Tortorici, A. L. Migdall, Y. Zhang, D. R. Kumor, W. H. Farr, F. Marsili, M. D. Shaw, J. A. Stern, C. Abellán, W. Amaya, V. Pruneri, T. Jennewein, M. W. Mitchell, P. G. Kwiat, J. C. Bienfang, R. P. Mirin, E. Knill, and S. W. Nam, Strong loophole-free test of local realism, Physical Review Letters **115**, 10.1103/physrevlett.115.250402 (2015).

[21] S. Storz, J. Schär, A. Kulikov, P. Magnard, P. Kurpiers, J. Lütolf, T. Walter, A. Copetudo, K. Reuer, A. Akin, J.-C. Besse, M. Gabureac, G. J. Norris, A. Rosario, F. Martin, J. Martinez, W. Amaya, M. W. Mitchell, C. Abellan, J.-D. Bancal, N. Sangouard, B. Royer, A. Blais, and A. Wallraff, Loophole-free bell inequality violation with superconducting circuits, Nature **617**, 265–270 (2023).

[22] G. C. Ghirardi, A. Rimini, and T. Weber, Unified dynamics for microscopic and macroscopic systems, Physical Review D **34**, 470–491 (1986).

[23] G. C. Ghirardi, P. Pearle, and A. Rimini, Markov processes in hilbert space and continuous spontaneous localization of systems of identical particles, Physical Review A **42**, 78–89 (1990).

[24] L. Diósi, Models for universal reduction of macroscopic quantum fluctuations, Physical Review A **40**, 1165–1174 (1989).

[25] P. Pearle, Reduction of the state vector by a nonlinear Schrödinger equation, Physical Review D **13**, 857 (1976).

[26] S. Weinberg, Testing quantum mechanics, Annals of Physics **194**, 336–386 (1989).

[27] N. Gisin, Stochastic quantum dynamics and relativity, Helv. Phys. Acta **62**, 363 (1989).

[28] J. Polchinski, Weinberg's nonlinear quantum mechanics and the einstein-podolsky-rosen paradox, Physical Review Letters **66**, 397–400 (1991).

[29] R. P. Feynman, Simulating physics with computers, International Journal of Theoretical Physics **21**, 467–488 (1982).

[30] W. Thomson, The tide gauge, tidal harmonic analyser, and tide predicter, Proc. Inst. Civil Engineers **65**, 3 (1881).

[31] P. J. Coles, C. Szczepanski, D. Melanson, K. Donatella, A. J. Martinez, and F. Sbahi, Thermodynamic ai and the fluctuation frontier, in *2023 IEEE International Conference on Rebooting Computing (ICRC)* (IEEE, 2023) p. 1–10.

[32] S. Duffield, M. Aifer, G. Crooks, T. Ahle, and P. J. Coles, Thermodynamic matrix exponentials and thermodynamic parallelism (2024), arXiv:2311.12759 [cond-mat.stat-mech].

[33] J. Chou, S. Bramhavar, S. Ghosh, and W. Herzog, Analog coupled oscillator based weighted ising machine, Scientific Reports **9**, 10.1038/s41598-019-49699-5 (2019).

[34] L. B. Kish, Quantum computing with analog circuits: Hilbert space computing, in *Smart Structures and Materials 2003: Smart Electronics, MEMS, BioMEMS, and Nanotechnology*, Vol. 5055, edited by V. K. Varadan and L. B. Kish (SPIE, 2003) p. 57.

[35] S. Mourya, B. R. L. Cour, and B. D. Sahoo, Emulation of quantum algorithms using cmos analog circuits, IEEE Transactions on Quantum Engineering **4**, 1 (2023).

[36] J. F. Muzzin, Analog simulation of the quantum bit (2024).

[37] J. W. M. Bush, V. Frumkin, and P. J. Sáenz, Perspectives on pilot-wave hydrodynamics, Applied Physics Letters **125**, 10.1063/5.0210055 (2024).

[38] P. Scherz and S. Monk, *Practical Electronics for Inventors*, 4th ed. (McGraw-Hill Education TAB, 2016).

[39] F. M. Mims, *Timer, Op Amp & Optoelectronic Circuits & Projects*, 4th ed. (Master Publishing, Inc., 2007).

[40] *Low Cost Analog Multiplier*, Analog Devices (2015).

[41] *LF411 FET-Input Operational Amplifier*, Texas Instruments (2025).

[42] R. P. Sallen and E. L. Key, A practical method of designing RC active filters, IRE Transactions on Circuit Theory **2**, 74 (1955).

[43] M. E. Van Valkenburg, *Analog Filter Design* (Holt, Rinehart and Winston, New York, 1982).

[44] J. R. Hance, S. Hossenfelder, and T. N. Palmer, Supermeasured: Violating bell-statistical independence without violating physical statistical independence, Foundations of Physics **52**, 10.1007/s10701-022-00602-9 (2022).

[45] N. Gisin, Weinberg's non-linear quantum mechanics and supraluminal communications, Phys. Lett. A **143**, 1 (1990).

[46] A. Valentini, Signal-locality in hidden-variables theories, Phys. Lett. A **297**, 273 (2002), arXiv:quant-ph/0106098.

[47] M. E. Bielińska, M. Eckstein, and P. Horodecki, Superluminal signalling and chaos in nonlinear quantum dynamics, New J. Phys. **27**, 053002 (2025).

[48] A. Patel and P. Kumar, Weak measurements, quantum-state collapse, and the born rule, Phys. Rev. A **96**, 022108 (2017).

[49] I. Siddiqi, S. J. Weber, K. W. Murch, A. Chantasri, J. Dressel, and A. N. Jordan, Observing single quantum trajectories of a superconducting qubit, in *Research in Optical Sciences*, QIM (OSA, 2014) p. QW1A.1.

[50] F. Anzà and J. P. Crutchfield, Beyond density matrices: Geometric quantum states, Phys. Rev. A **103**, 062218 (2021).

[51] S. Das and J. R. Green, Density matrix formulation of dynamical systems, Phys. Rev. E **106**, 054135 (2022).

[52] S. Das and J. R. Green, Speed limits on deterministic chaos and dissipation, Phys. Rev. Res. **5**, L012016 (2023).

[53] S. H. Strogatz, *Nonlinear Dynamics and Chaos: With Applications to Physics, Biology, Chemistry, and Engineering*, 2nd ed., Studies in Nonlinearity (Westview Press, 2014).

[54] A. Montina, Exponential complexity and ontological theories of quantum mechanics, Phys. Rev. A **77**, 022104 (2008).

[55] A. Montina, State-space dimensionality in short-memory hidden-variable theories, Phys. Rev. A **83**, 032107 (2011).

[56] B. Skinner, J. Ruhman, and A. Nahum, Measurement-induced phase transitions in the dynamics of entanglement, Phys. Rev. X **9**, 031009 (2019).

[57] C. Noel, P. Niroula, D. Zhu, A. Risinger, L. Egan, D. Biswas, M. Cetina, A. V. Gorshkov, M. J. Gullans, D. A. Huse, and C. Monroe, Measurement-induced quantum phases realized in a trapped-ion quantum computer,

Nat. Phys. **18**, 760 (2022).